Journal of Computational Physics 392 (2019) 161–186

Contents lists available at ScienceDirect

Journal of Computational Physics

www.elsevier.com/locate/jcp

Staggered-grid entropy-stable multidimensional summation-by-parts discretizations on curvilinear coordinates ☆

David C. Del Rey Fernández [a,b,*], Jared Crean [c], Mark H. Carpenter [b], Jason E. Hicken [c]

[a] National Institute of Aerospace, Hampton, VA, United States
[b] Computational AeroSciences Branch, NASA Langley Research Center, Hampton, VA, United States
[c] Department of Mechanical, Aerospace, and Nuclear Engineering, Rensselaer Polytechnic Institute, Troy, NY, United States

ARTICLE INFO

Article history:
Received 15 September 2018
Received in revised form 20 March 2019
Accepted 13 April 2019
Available online 24 April 2019

Keywords:
Nonlinear entropy stability
Summation-by-parts
Simultaneous approximation terms
High-order discretizations
General elements and curved elements
Unstructured grid

ABSTRACT

The entropy conservative/stable staggered grid tensor-product algorithm of Parsani et al. [1] is extended to multidimensional SBP discretizations. The required SBP preserving interpolation operators are proven to exist under mild restrictions and the resulting algorithm is proven to be entropy conservative/stable as well as elementwise conservative. For 2-dimensional simplex elements, the staggered grid algorithm is shown to be more accurate and have a larger maximum time step restriction as compared to the collocated algorithm. The staggered algorithm significantly reduces the number of (computationally expensive) two-point flux evaluations, which is potentially important for both explicit and implicit time-marching schemes. Furthermore, the staggered algorithm requires fewer degrees of freedom for comparable accuracy, which has favorable implications for implicit time-marching schemes.

1. Introduction

Efficient numerical algorithms are sought that exploit $\mathcal{O}(10^9)$ exascale concurrency on next generation hardware. Clearly, hardware compatibility and efficiency are of paramount importance in determining an algorithm's viability at exascale. Equally important (if not more so) is algorithmic robustness, which becomes progressively more difficult to achieve as problem size increases.

High-order FEM methods provide an efficient approach to achieve high solution accuracy. They are amenable to H-, P-, and R-refinement algorithms, and have computational kernels that are arithmetically dense making them compatible with highly concurrent hardware. Recently, nonlinearly stable, (entropy stable) high-order FEM algorithms have been developed for the compressible Navier-Stokes equations [1–4]. Thus, high-order, entropy stable FEM algorithms are well positioned for the challenges of exascale.

☆ D. Del Rey Fernández was partially supported by a NSERC Postdoctoral Fellowship, J. Crean was supported by the National Science Foundation under Grant No. 1554253, and J. Hicken was partially funded by the Air Force Office of Scientific Research Award FA9550-15-1-0242 under Dr. Jean-Luc Cambier. The authors gratefully acknowledge this support.

* Corresponding author at: Computational AeroSciences Branch, NASA Langley Research Center, Hampton, VA, United States.
E-mail addresses: dcdelrey@gmail.com (D.C. Del Rey Fernández), jcrean01@gmail.com (J. Crean), mark.h.carpenter@nasa.gov (M.H. Carpenter), hickej2@rpi.edu (J.E. Hicken).

https://doi.org/10.1016/j.jcp.2019.04.029
0021-9991/

High-order methods are known to be more efficient than low-order methods for linear wave propagation [5,6]. However, without provable stability, their use can be hampered by lack of robustness. Nevertheless, a systematic procedure for constructing linearly stable schemes of arbitrary order is available within the summation-by-parts (SBP) framework (see the survey papers [7,8]). SBP operators are matrix difference operators that discretely mimic continuous integration-by-parts. As an example, an SBP matrix difference operator used to approximate the x derivative is generically given as

$$\mathsf{D}_x \equiv \mathsf{H}^{-1}\mathsf{Q}_x,$$

where the symmetric and skew-symmetric parts of Q_x are denoted $\frac{1}{2}\mathsf{E}_x$ and S_x, respectively. The constituent matrices of an SBP operator (H, Q_x, E_x) are high-order approximations to continuous bilinear forms, i.e., for grid functions $\boldsymbol{v}$ and $\boldsymbol{u}$ (constructed from continuous function $\mathcal{V}$ and $\mathcal{U}$)

$$\boldsymbol{v}^{\mathrm{T}}\mathsf{H}\boldsymbol{u} \approx \int_{\Omega} \mathcal{V}\mathcal{U}\mathrm{d}\Omega, \qquad \boldsymbol{v}^{\mathrm{T}}\mathsf{Q}_x\boldsymbol{u} \approx \int_{\Omega} \mathcal{V}\frac{\partial \mathcal{U}}{\partial x}\mathrm{d}\Omega, \qquad \boldsymbol{v}^{\mathrm{T}}\mathsf{E}_x\boldsymbol{u} \approx \oint_{\Gamma} \mathcal{V}\mathcal{U}n_x\mathrm{d}\Gamma,$$

where n_x is the x component of the unit normal. Using these relations, SBP operators can be shown to mimic integration by parts to high order term-by-term, i.e.,

$$\begin{array}{ccccc} \underbrace{\boldsymbol{v}^{\mathrm{T}}\mathsf{Q}_x\boldsymbol{u}} & + & \underbrace{\boldsymbol{u}^{\mathrm{T}}\mathsf{Q}_x\boldsymbol{v}} & = & \underbrace{\boldsymbol{v}^{\mathrm{T}}\mathsf{E}_x\boldsymbol{u}} \\ \approx \int_{\Omega} \mathcal{V}\frac{\partial \mathcal{U}}{\partial x}\mathrm{d}\Omega & & \approx \int_{\Omega} \mathcal{U}\frac{\partial \mathcal{V}}{\partial x}\mathrm{d}\Omega & & \approx \oint_{\Gamma} \mathcal{V}\mathcal{U}n_x\mathrm{d}\Gamma \end{array}.$$

It is this mimetic property that enables the construction of linearly stable schemes of arbitrary order. Interface operators and boundary conditions that are compatible with SBP operators are also available, (e.g., simultaneous approximation terms (SATs) [9–13]), as are stable operators for linear variable coefficient problems [12].

The relative success of high-order, provably stable algorithms for linear problems motivates the search for high-order provably stable methods for nonlinear problems. Tadmor [14], in a pioneering effort, constructed nonlinearly stable second-order finite-volume schemes for the compressible Euler equations in one spatial dimension. Nonlinear stability was achieved by discretely mimicking continuous entropy conservation through the use of conservative numerical two-point flux functions that, when contracted with the entropy variables, result in a telescoping potential flux; stability is then achieved by introducing appropriate dissipation. This telescoping property allows the semidiscrete stability analysis to mimic the continuous L^2 entropy stability analysis (for a review of these ideas see Tadmor [15]). Such schemes have been extended to high-order ENO by Fjordholm et al. [16] and low-order unstructured finite volume discretizations by Ray et al. [17], to name a few developments in this community.

Fisher and coauthors provide a generalization of Tadmor's two-point flux function procedure. By combining Tadmor's 2nd-order mechanics with the SBP framework, entropy conservative operators of arbitrary order can be constructed. The initial synthesis appears in a series of papers within the context of classical finite-difference SBP discretizations [18–20]. These ideas have since been extended to include collocated spectral elements [2], multidimensional SBP operators [3,4], modal methods using decoupled SBP operators [21], as well as to a number of PDEs besides the Euler and Navier-Stokes equations (for example MHD [22–24] and shallow water [25–27]). The combination of SBP operators and two-point flux functions is attractive because it inherits all of the mechanics of linear SBP schemes for the imposition of boundary conditions and interelement coupling and thereby gives a systematic methodology for discretizing problems on complex geometries. Moreover, constructing schemes that discretely mimic a continuous stability proof naturally produces semi-discrete or fully-discrete [28] schemes that inherit an L^2 entropy stability estimate; there is no need to assume exact integration, as is commonly done in alternative approaches [29,30].

Herein, entropy stable operators based on the multidimensional SBP framework are developed that are suitable for general nodal distributions that arise in tetrahedra, prisms, and pyramids. Efficient operators are critical for these element types because they are ubiquitous in the unstructured meshes frequently used by practitioners. Entropy-stable schemes for the compressible Euler equations that use multidimensional SBP operators have been previously developed. (See Crean et al. [4] for results on triangles and tetrahedra, and Chen and Shu [3] for results on triangles.) As will be shown, however, these operators have several undesirable attributes that can be easily mitigated using the present approach.

Collocated multidimensional SBP operators can be delineated into two categories: those constructed with dense E and those with diagonal E (see Fig. 1). Dense-E SBP operators can be constructed using minimal (or nearly minimal) nodal sets on triangles and tetrahedra for all practical orders [4]. Entropy conservative operators constructed with dense-E require interface coupling SATs that fully couple adjoining elements. Consequently, the extensive element-to-element coupling makes entropy conservative/stable schemes computationally expensive, in this case, because of the excessive number of two-point flux evaluations required to ensure entropy conservation. Alternatively, SBP operators with diagonal-E are constructed on nodal sets that include both interior and surface nodes [3,4], in order to accommodate design order surface cubatures. These additional constraints, however, force the dimension of diagonal-E nodal sets to be suboptimal. For example, at polynomial orders $(1, 2, 3, 4)$, the ratio of the nodal dimension between dense and diagonal-E nodal sets are

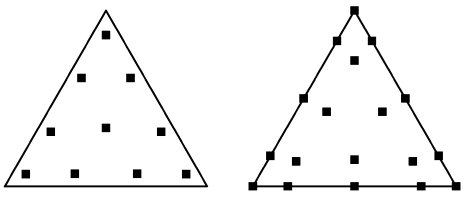

(a) Dense-E ($p = 3$). (b) Diagonal-E ($p = 3$).

Fig. 1. Example nodal distributions.

$n \in (3/6, 6/12, 10/18, 15/27)$ for triangles, and $(4/13, 10/36, 20/69, 38/99)$ for tetrahedra, where n is the number of nodes. Note that the number of nodes for dense-E SBP operators is optimal for triangles $[(p+1)(p+2)/2]$ and nearly optimal for tetrahedra $[(p+1)(p+2)(p+3)/6]$, where p is the degree of the operator. Despite having nearly twice (or thrice) the nodal dimension for triangles (or tetrahedra), the number of two-point flux evaluations is vastly reduced with diagonal-E SBP operators because adjoining elements only couple on their surfaces ($\mathcal{O}(n^2)$ vs. $\mathcal{O}(n^6)$). In addition, the mechanics for constructing entropy stable numerical boundary conditions are well understood for diagonal-E operators while it is still unclear how to proceed for dense-E operators. Diagonal-E operators are currently preferred when constructing entropy stable operators on triangles and tetrahedra [3,4].

Clearly, minimizing problem size per unit accuracy is (nearly) always desirable. Some applications, however, are much more sensitive to excess degrees of freedom (DOFs); implicit temporal advancement being an example. External aerodynamic solvers typically use implicit temporal advancement algorithms to cope with the stiffness resulting from high aspect ratio boundary layer elements. Implicit algorithms require repeated solutions of linear/nonlinear algebraic systems at each stage/timestep, with the dimension scaling linearly with the number of cubature nodes, for collocated methods, since DOFs are one-to-one with the number of cubature nodes. Countless techniques exist for solving the linear systems resulting from the linearization of FEM operators, although all depend strongly on the number of DOFs. For example, on-element block Jacobi preconditioners require a local matrix inverse (direct or iterative), that at worst can scale cubically with the number of on-element cubature points. Thus, dense-E on minimal nodal sets are an attractive option for implicit time advancement methods (assuming comparable accuracy as with the suboptimal alternatives). If only there was a way to combine interior and boundary operators to exploit the desirable attributes of each!

Parsani et al. [1] recently proposed a staggered grid approach for tensor-product operators based on dense-E and diagonal-E nodal sets. The solution was stored and advanced in time on a dense-E nodal set (tensor product Gauss Legendre points), while the inviscid (and viscous) volume and surface fluxes where computed on a diagonal-E nodal set (tensor product Legendre-Gauss-Lobatto points). The staggered algorithm was significantly more accurate than a collocated operator, the result of an "over-integration" effect. Furthermore, the number of two-point function evaluations was greatly reduced relative to a tensor product Gauss Legendre operator.

The present work generalizes the work of Parsani et al. [1] to multidimensional SBP operators. A staggered combination of dense-E and diagonal-E nodes is used such that the desirable features of each approach are realized. The solution is stored on a nodal set, which is minimal, or nearly minimal, in cardinality. The volume and surface integrations are carried out on a nodal set associated with a diagonal-E SBP operator. Thus, although the problem size is nearly optimal, the surface cubatures only couple surface points between adjoining elements, thereby minimizing the number of two-point flux evaluations. Interpolation operators that satisfy a precise prolongation/restriction relation are used to maintain the SBP properties and thereby ensure nonlinear entropy stability of the staggered operator.

A summary of the contributions for this work includes the following: 1) prolongation/restriction pairs are shown to exist between dense-and diagonal-E nodal sets under very mild assumptions. 2) staggered multidimensional SBP operators are shown to be more accurate than diagonal-E SBP operators although the DOFs are reduced by a factor of 2 (or 3) for triangles (or tetrahedra). 3) the right-hand-side residual evaluation is identical for the staggered operator and the diagonal-E operator. Thus, Euler equation timings for explicit time advancement algorithms is nearly equivalent for the two approaches (in Parsani et al. the diagonal-E node set was taken as the Legendre-Gauss-Lobatto nodes at one degree higher than necessary). 4) the staggered operator results in a larger explicit stability limit as compared to the diagonal-E operator.

The paper is organized as follows: in Section 2, we delineate the notation used in the paper, a few definitions, and review multidimensional SBP operators. Next, we give a brief review of the continuous entropy stability analysis in Section 3. Existence and the construction of SBP-preserving interpolation operators (necessary for the staggered scheme that we develop) are detailed in Section 4. The staggered-grid discretization of the Euler equations is presented in Section 5, while entropy conservation is proven in Section 5.1. We prove that our semidiscrete scheme is elementwise conservative in Section 5.2 and present how to construct appropriate interface dissipation to achieve entropy stability in Section 5.3. The theoretical properties of the scheme are numerically verified in Section 6 and, in addition, some preliminary cost comparisons are performed. Finally, conclusions are draw in Section 7.

2. Notation, definitions, and review of multidimensional SBP operators

Consider a compact connected set $\Omega \subset \mathbb{R}^3$ in Cartesian coordinates $(x_1, x_2, x_3) \subset \mathbb{R}^3$. Let the boundary of Ω be denoted by Γ, where it is assumed that Γ is piecewise smooth. We use a domain decomposition strategy and therefore, partition Ω into a set of K nonoverlapping elements. The domain of the κth element is denoted by Ω_κ and its boundary by Γ_κ; therefore, $\Omega = \bigcup_{\kappa=1}^{K} \Omega_\kappa$. Rather than discretizing PDEs in Cartesian coordinates, they are discretized in curvilinear coordinates $(\xi_1, \xi_2, \xi_3) \subset \mathbb{R}^3$; each Ω_κ is locally transformed to $\hat{\Omega}_\kappa$ under the following assumption (i.e., the computational reference space, for example, in this paper is the equilateral tetrahedron):

Assumption 1. Each element in physical space is transformed using local invertible curvilinear coordinate transformations that are compatible at shared interfaces, meaning that points in computational space on either side of the shared surface are mapped to the same physical location and therefore map back to the analogous location in computational space.

We deal with generic element types that have a finite number of smooth subsurfaces, and it is therefore convenient to introduce the following notation:

$$\sum_{\gamma \subset \Gamma_\kappa} (\cdot),$$

which is used to indicate a sum over all smooth subsets of Γ_κ. In practice, γ is an individual (smooth) face for which a cubature rule can be defined.

Functions on a particular domain are represented using a script type and bold font is used for vector-valued functions. As an example, $\mathcal{U} \in L^2(\Omega)$ is a square integrable function on Ω, while $\boldsymbol{\mathcal{F}} \in \left[L^2(\Omega_\kappa)\right]^5$ is a 5-vector-valued function having square integrable components on the element Ω_κ. We will reserve $\mathcal{P}$, $\mathcal{Q} \in \mathbb{P}_d(\Omega)$ for polynomials, where $\mathbb{P}_d(\Omega)$ is the space of polynomials of total degree d on Ω.

Functions are discretized using their nodal values at points within elements and possibly at their boundaries. Thus, if the κth element has n_κ nodes given by $C_\kappa \equiv \left\{(\xi_1^i, \xi_2^i, \xi_3^i)\right\}_{i=1}^{n_\kappa} = \left\{\boldsymbol{\xi}_i\right\}_{i=1}^{n_\kappa}$, then the function $\mathcal{U}$ evaluated at these nodes is represented by the column vector

$$\boldsymbol{u} \equiv \left[\mathcal{U}\left(\boldsymbol{\xi}_1\right), \quad \ldots \quad, \mathcal{U}\left(\boldsymbol{\xi}_{n_\kappa}\right)\right]^{\mathrm{T}}.$$

The symbols $\mathbf{1}$ and $\mathbf{0}$ denote vectors consisting of all ones and all zeros, respectively. The number of entries in $\mathbf{1}$ and $\mathbf{0}$ can always be inferred from the context. We will reserve $\boldsymbol{p}$ and $\boldsymbol{q}$ for the generic polynomials $\mathcal{P}$ and $\mathcal{Q}$ evaluated at the points in C_κ.

Matrices are represented with an uppercase sans serif type, for example $\mathsf{A} \in \mathbb{R}^{n \times m}$. The $n \times n$ identity matrix is represented by I_n. The Kronecker product is used to extend scalar differentiation matrices to vector differentiation matrices and is given in the following definition:

Definition 1. The Kronecker product between the matrix $\mathsf{A} \in \mathbb{R}^{n \times m}$ and $\mathsf{B} \in \mathbb{R}^{p \times q}$ is denoted by

$$\mathsf{A} \otimes \mathsf{B} \equiv \begin{bmatrix} a_{1,1}\mathsf{B} & \ldots & a_{1,m}\mathsf{B} \\ \vdots & & \vdots \\ a_{n,1}\mathsf{B} & \ldots & a_{n,m}\mathsf{B} \end{bmatrix},$$

and has the following useful properties:

- $(\mathsf{A} \otimes \mathsf{B})^{\mathrm{T}} = \mathsf{A}^{\mathrm{T}} \otimes \mathsf{B}^{\mathrm{T}}$
- $(\mathsf{A} \otimes \mathsf{B})^{-1} = \mathsf{A}^{-1} \otimes \mathsf{B}^{-1}$
- if the products AC and BD exist then $(\mathsf{A} \otimes \mathsf{B})(\mathsf{C} \otimes \mathsf{D}) = \mathsf{AC} \otimes \mathsf{BD}$

The Hadamard product will be used in the construction of entropy conservative/stable discretizations and is defined by

Definition 2. The Hadamard product between the matrix $\mathsf{A} \in \mathbb{R}^{n \times n}$ and $\mathsf{B} \in \mathbb{R}^{n \times n}$ is denoted by

$$\mathsf{A} \circ \mathsf{B} \equiv \begin{bmatrix} a_{11}b_{11} & \ldots & a_{1n}b_{1n} \\ \vdots & & \vdots \\ a_{n1}b_{n1} & \ldots & a_{nn}b_{nn} \end{bmatrix},$$

and has the useful properties

$$\mathsf{A} \circ \mathsf{B} = \mathsf{B} \circ \mathsf{A},$$
$$\mathsf{A} \circ (\mathsf{B} \circ \mathsf{C}) = (\mathsf{A} \circ \mathsf{B}) \circ \mathsf{C},$$
$$\mathsf{A} \circ (\mathsf{B} + \mathsf{C}) = \mathsf{A} \circ \mathsf{B} + \mathsf{A} \circ \mathsf{C},$$
$$(\mathsf{A} \circ \mathsf{B})^{\mathrm{T}} = \mathsf{A}^{\mathrm{T}} \circ \mathsf{B}^{\mathrm{T}}.$$

SBP operators are matrix difference operators approximating derivatives at discrete nodal locations and are given by [31]

Definition 3 *(Summation-by-parts operator).* The matrix D_{ξ_l} is a degree p SBP approximation to the first derivative $\frac{\partial}{\partial \xi_l}$ on the nodes $C_\kappa = \{\boldsymbol{\xi}_i\}_{i=1}^{n_\kappa}$ if

1. $\mathsf{D}_{\xi_l}\boldsymbol{p}$ is equal to $\partial \mathcal{P}/\partial \xi_l$ at the nodes C_κ, for all polynomials $\mathcal{P} \in \mathbb{P}_p(\hat{\Omega}_\kappa)$;
2. $\mathsf{D}_{\xi_l} = \mathsf{H}^{-1}\mathsf{Q}_{\xi_l}$, where H is symmetric positive-definite, and;
3. $\mathsf{Q}_{\xi_l} = \mathsf{S}_{\xi_l} + \frac{1}{2}\mathsf{E}_{\xi_l}$, where $\mathsf{S}_{\xi_l}^T = -\mathsf{S}_{\xi_l}$, $\mathsf{E}_{\xi_l}^T = \mathsf{E}_{\xi_l}$, and E_{ξ_l} satisfies

$$\boldsymbol{p}^T \mathsf{E}_{\xi_l} \boldsymbol{q} = \int_{\hat{\Gamma}_\kappa} \mathcal{P}\, \mathcal{Q}\, n_{\xi_l} \mathrm{d}\hat{\Gamma},$$

for all polynomials $\mathcal{P}, \mathcal{Q} \in \mathbb{P}_r(\hat{\Omega}_\kappa)$, where $r \geq p$. In the above integral, n_{ξ_l} is the ξ_l component of $\boldsymbol{n} = \left[n_{\xi_1}, n_{\xi_2}, n_{\xi_3}\right]^T$, the outward pointing unit normal on $\hat{\Gamma}_\kappa$.

Remark 1. In this paper, we deal with diagonal-norm SBP operators, for which H is a diagonal matrix with strictly positive entries. In this case, the nodes C_κ and entries in H define a cubature that is exact for polynomials of degree $2p-1$, at least [31].

We couple adjacent elements using SATs [9–13], which can be thought of as interior penalty terms. As in the case of one-dimensional SBP operators [32], it is convenient to decompose the E_{ξ_l} into contributions from subfaces on $\hat{\Gamma}_\kappa$. Here we follow the approach in [4,33,34] and construct E_{ξ_l} from interpolation/extrapolation operators that interpolate/extrapolate the solution from the SBP nodes to nodes on the elements boundary.

Consider the κth element, and let $\gamma \subset \hat{\Gamma}_\kappa$ be one of its smooth faces. Furthermore, let $C_\gamma \equiv \{\boldsymbol{\xi}_i\}_{i=1}^{n_\gamma} \subset \gamma$ be a set of cubature nodes with positive weights $\{b_i\}_{i=1}^{n_\gamma}$ exact for polynomials of total degree $2r$. Then, if the degree r Vandermonde matrix (see Definition 4) associated with C_γ has full column rank, we can construct the degree r interpolation/extrapolation operator $\mathsf{R}_{\gamma\kappa} \in \mathbb{R}^{n_\gamma \times n_\kappa}$ from the nodes C_κ to the nodes C_γ, i.e., [33]

$$\left(\mathsf{R}_{\gamma\kappa}\boldsymbol{p}\right)_j = \sum_{i=1}^{n_\kappa} (\mathsf{R}_{\gamma\kappa})_{ji} \mathcal{P}\left(\boldsymbol{\xi}_i\right) = \mathcal{P}\left(\boldsymbol{\xi}_j\right), \qquad \forall\, j = 1, \ldots, n_\gamma, \quad \forall\, \mathcal{P} \in \mathbb{P}_r\left(\hat{\Omega}_\kappa\right).$$

The degree p Vandermonde matrix is defined by

Definition 4. The degree p Vandermonde matrix on a set of nodes $C_\kappa = \{\boldsymbol{\xi}_i\}_{i=1}^{n_\kappa}$ with respect to the basis functions $\mathcal{P}_i \in \mathbb{P}_p$ is the matrix

$$\mathsf{V}(:, i) = \boldsymbol{p}_i, \quad i = 1, 2, \ldots \binom{p+d}{d},$$

where $\boldsymbol{p}_i$ is the ith basis function evaluated at the nodes C_κ and d is the dimension of the space in which C_κ exists (in our case $d = 3$ and so $\binom{p+d}{d} = (p+3)(p+2)(p+1)/6$).

Remark 2. We could use any convenient set of basis functions in the construction of the Vandermonde matrix, for example the monomials, however, in practice this could lead to ill-conditioning during the construction of the operators considered later. Therefore, in this paper, we use the Proriol polynomials, which are mutually orthogonal on the triangle.

The E_{ξ_l} matrices in Definition 3 can be constructed from the interpolation/extrapolation operators for each γ as [33]

$$\mathsf{E}_{\xi_l} = \sum_{\gamma \subset \partial\hat{\Omega}_\kappa} \mathsf{E}_{\xi_l}^{\gamma,\kappa}, \qquad \text{where} \qquad \mathsf{E}_{\xi_l}^{\gamma,\kappa} \equiv \mathsf{R}_{\gamma\kappa}^{\mathrm{T}} \mathsf{N}_{\xi_l,\gamma} \mathsf{B}_\gamma \mathsf{R}_{\gamma\kappa}, \tag{1}$$

where $\mathsf{B}_\gamma = \mathrm{diag}(b_1, b_2, \ldots, b_{n_\gamma})$ is a diagonal matrix whose entries are the positive cubature weights for face γ, and $\mathsf{N}_{\xi_l,\gamma} = \mathrm{diag}\left[\left(n_{\xi_l}\right)_1, \left(n_{\xi_l}\right)_2, \ldots, \left(n_{\xi_l}\right)_{n_\gamma}\right]$ is a diagonal matrix whose entries are the ξ_l component of the unit outward normal

to $\hat{\Gamma}_\kappa$ at the cubature points of face γ. There exists at least one SBP operator whose E_{ξ_l} has the decomposition (1) for a given C_κ and H [33], and we assume that such an SBP operator is used throughout this work.

We also use interpolation/extrapolation operators to define the coupling matrices, which are used to couple adjacent elements:

$$\mathsf{E}^{\kappa,\nu}_{\xi_l,m,\gamma} \equiv \mathsf{R}^{\mathrm{T}}_{\gamma\kappa}\mathsf{A}^{l,m}_{\gamma}\mathsf{N}_{\xi_l,\gamma}\mathsf{B}_\gamma\mathsf{R}_{\gamma\nu}, \qquad \mathsf{E}^{\nu,\kappa}_{\xi_l,m,\gamma} = -\left(\mathsf{E}^{\kappa,\nu}_{\xi_l,m,\gamma}\right)^{\mathrm{T}}, \tag{2}$$

where $\mathsf{A}^{l,m}_{\gamma}$ is a diagonal matrix with the metric term $\mathcal{J}\frac{\partial \xi_l}{\partial x_m}$ evaluated at the cubature nodes of surface γ, that is

$$\mathsf{A}^{l,m}_{\gamma} = \mathrm{diag}\left[\mathcal{J}\frac{\partial \xi_l}{\partial x_m}(\boldsymbol{\xi}_1), \ldots, \mathcal{J}\frac{\partial \xi_l}{\partial x_m}(\boldsymbol{\xi}_{n_\gamma})\right],$$

where $\mathrm{diag}(\boldsymbol{v})$ is a diagonal matrix with its diagonal entries populated by the components of $\boldsymbol{v}$. Note that when the matrices (1) and (2) are left and right multiplied by grid functions, they approximate surface integrals, that is

$$\boldsymbol{p}^{\mathrm{T}}\mathsf{E}_{\xi_l}\boldsymbol{q} \approx \oint_{\hat{\Gamma}_\kappa} \mathcal{P}\mathcal{Q}n_{\xi_l}\mathrm{d}\hat{\Gamma}, \quad \boldsymbol{p}^{\mathrm{T}}\mathsf{E}^{\kappa,\nu}_{\xi_l,m,\gamma}\boldsymbol{q} \approx \oint_{\gamma} \mathcal{P}\mathcal{Q}n_{\xi_l}\mathrm{d}\hat{\Gamma}.$$

Remark 3. We will assume that the normal is outward pointing with respect to κ in the adjacent pair of generic elements κ and ν.

3. Review of entropy stability

3.1. Governing equations

In this work, we will construct entropy conservative/stable discretizations of the Euler equations for a calorically perfect gas, which in Cartesian coordinates and in three-dimensions are given as

$$\frac{\partial \boldsymbol{\mathcal{U}}}{\partial t} + \sum_{m=1}^{3}\frac{\partial \boldsymbol{\mathcal{F}}_m}{\partial x_m} = \boldsymbol{0}, \qquad \forall\, \boldsymbol{x} \in \Omega, \tag{3}$$

where well-posed data is assumed (we forgo a detailed description of the Euler equations as this can be found elsewhere, for example LeVeque [35]).

We transform (3) on each Ω_κ into curvilinear coordinates and recast the resulting PDE into an average of the conservative and chain-rule forms, giving

$$\frac{\partial \mathcal{J}_\kappa \boldsymbol{\mathcal{U}}_\kappa}{\partial t} + \sum_{l,m=1}^{3}\frac{1}{2}\frac{\partial \mathcal{A}^{l,m}_\kappa \boldsymbol{\mathcal{F}}_m}{\partial \xi_l} + \frac{\mathcal{A}^{l,m}_\kappa}{2}\frac{\partial \boldsymbol{\mathcal{F}}_m}{\partial \xi_l} = \boldsymbol{0}, \tag{4}$$

where $\mathcal{J}_\kappa$ is the local metric Jacobian and we have used the metric identities

$$\sum_{l=1}^{3}\frac{\partial \mathcal{A}^{l,m}_\kappa}{\partial \xi_l} = 0, \qquad \mathcal{A}^{l,m}_\kappa \equiv \mathcal{J}_\kappa\frac{\partial \xi_l}{\partial x_m}, \qquad m = 1,2,3. \tag{5}$$

3.2. Continuous entropy analysis

The compressible Euler equations, given in form (3) or (4), have a convex extension of their original form, that when integrated over the physical domain Ω, or piecewise over the computational domains $\hat{\Omega}_\kappa$, depend only on the boundary data. This convex extension results in an entropy function that provides a mechanism for proving stability in the L^2 norm. Indeed, Dafermos [36] proved that if a system of conservation laws is endowed with a convex entropy function, $\mathcal{S} = \mathcal{S}(\boldsymbol{\mathcal{U}})$, then a bound on the global estimate of $\mathcal{S}$ can be converted into an a priori estimate on the solution vector $\boldsymbol{\mathcal{U}}$ (see also Svärd [37]).

Definition 5. A scalar function $\mathcal{S} = \mathcal{S}(\boldsymbol{\mathcal{U}})$ is an entropy function of a system of conservation laws if it satisfies the following conditions:

- In Cartesian coordinates, the gradient of the convex function $\mathcal{S}(\boldsymbol{\mathcal{U}})$, with respect to the conservative variables, simultaneously contracts all of the spatial fluxes as follows:

$$\frac{\partial \mathcal{S}}{\partial \boldsymbol{\mathcal{U}}}\frac{\partial \boldsymbol{\mathcal{F}}_m}{\partial x_m} = \frac{\partial \mathcal{S}}{\partial \boldsymbol{\mathcal{U}}}\frac{\partial \boldsymbol{\mathcal{F}}_m}{\partial \boldsymbol{\mathcal{U}}}\frac{\partial \boldsymbol{\mathcal{U}}}{\partial x_m} = \frac{\partial \mathcal{F}_m}{\partial \boldsymbol{\mathcal{U}}}\frac{\partial \boldsymbol{\mathcal{U}}}{\partial x_m} = \frac{\partial \mathcal{F}_m}{\partial x_m}, \qquad m = 1, 2, 3.$$

The components of the contracting vector $\partial \mathcal{S}/\partial \boldsymbol{\mathcal{U}}$, are the entropy variables and are denoted by the vector $\boldsymbol{\mathcal{W}}^{\mathrm{T}} = \partial \mathcal{S}/\partial \boldsymbol{\mathcal{U}}$. Furthermore, the scalars $\mathcal{F}_m(\boldsymbol{\mathcal{U}})$ are the entropy fluxes in the m-direction.

- If $\boldsymbol{\mathcal{W}}$ takes the role of a new set of independent variables, i.e., $\boldsymbol{\mathcal{U}} = \boldsymbol{\mathcal{U}}(\boldsymbol{\mathcal{W}})$, then the entropy variables symmetrize their associated system of conservation laws. For example, the Euler equations expressed in terms of the entropy variables yields

$$\frac{\partial \boldsymbol{\mathcal{U}}}{\partial t} + \sum_{m=1}^{3}\frac{\partial \boldsymbol{\mathcal{F}}_m}{\partial x_m} = \frac{\partial \boldsymbol{\mathcal{U}}}{\partial \boldsymbol{\mathcal{W}}}\frac{\partial \boldsymbol{\mathcal{W}}}{\partial t} + \sum_{m=1}^{3}\frac{\partial \boldsymbol{\mathcal{F}}_m}{\partial \boldsymbol{\mathcal{W}}}\frac{\partial \boldsymbol{\mathcal{W}}}{\partial x_m} = 0,$$

where $\partial \boldsymbol{\mathcal{U}}/\partial \boldsymbol{\mathcal{W}} = (\partial \boldsymbol{\mathcal{U}}/\partial \boldsymbol{\mathcal{W}})^{\mathrm{T}}$ and $\partial \boldsymbol{\mathcal{F}}_m/\partial \boldsymbol{\mathcal{W}} = (\partial \boldsymbol{\mathcal{F}}_m/\partial \boldsymbol{\mathcal{W}})^{\mathrm{T}}$, since the entropy is convex, the Hessian $\partial^2 \mathcal{S}/\partial \boldsymbol{\mathcal{U}}^2$ is symmetric positive definite,

$$\boldsymbol{\mathcal{V}}^{\mathrm{T}}\frac{\partial^2 \mathcal{S}}{\partial \boldsymbol{\mathcal{U}}^2}\boldsymbol{\mathcal{V}} > 0, \qquad \forall\, \boldsymbol{\mathcal{V}} \neq 0,$$

and yields a one-to-one mapping from conservative variables, $\boldsymbol{\mathcal{U}}$, to entropy variables, $\boldsymbol{\mathcal{W}}$. Similarly, $\partial \boldsymbol{\mathcal{U}}/\partial \boldsymbol{\mathcal{W}}$ is symmetric positive definite, since it is the inverse of $\partial^2 \mathcal{S}/\partial \boldsymbol{\mathcal{U}}^2$. The entropy and corresponding entropy flux are denoted an entropy-entropy flux pair, $(\mathcal{S}, \mathcal{F}_m)$ [15].
The fact that the matrices $\partial \boldsymbol{\mathcal{U}}/\partial \boldsymbol{\mathcal{W}}$ and $\partial \boldsymbol{\mathcal{F}}_m/\partial \boldsymbol{\mathcal{W}}$ are symmetric indicates that the conservative variables, $\boldsymbol{\mathcal{U}}$, and the fluxes, $\boldsymbol{\mathcal{F}}_m$, are Jacobians of scalar functions with respect to the entropy variables, i.e.,

$$\boldsymbol{\mathcal{U}}^{\mathrm{T}} = \frac{\partial \Phi}{\partial \boldsymbol{\mathcal{W}}}, \quad \boldsymbol{\mathcal{F}}_m^{\mathrm{T}} = \frac{\partial \Psi_m}{\partial \boldsymbol{\mathcal{W}}},$$

where, Φ, is called the potential and the Ψ_m are called the potential fluxes [15] and are denoted as a potential-potential flux pair, (Φ, Ψ_m) [15]. In the same way that the entropy function is convex with respect to the conservative variables, i.e., $\partial^2 \mathcal{S}/\partial \boldsymbol{\mathcal{U}}^2$ is symmetric positive definite, the potential function is convex with respect to the entropy variables.

There is a close relation between the entropy and the potential and their associated fluxes, as shown by Godunov [38] and Mock [39]. In particular, Godunov proves

Theorem 1. *If a system of conservation laws can be symmetrized by introducing new variables $\boldsymbol{\mathcal{W}}$, and $\boldsymbol{\mathcal{U}}$ is a convex function of Φ, then an entropy function $\mathcal{S} = \mathcal{S}(\boldsymbol{\mathcal{U}})$ is given by*

$$\Phi = \boldsymbol{\mathcal{W}}^{\mathrm{T}}\boldsymbol{\mathcal{U}} - \mathcal{S}, \tag{6}$$

and the entropy fluxes $\mathcal{F}_m(\boldsymbol{\mathcal{U}})$ satisfy

$$\Psi_m = \boldsymbol{\mathcal{W}}^{\mathrm{T}}\boldsymbol{\mathcal{F}}_m - \mathcal{F}_m. \tag{7}$$

Proof. The proof of this theorem can be found in references [38,40]. □

Mock proves the converse to be true:

Theorem 2. *If $\mathcal{S} = \mathcal{S}(\boldsymbol{\mathcal{U}})$ is an entropy function of a system of conservation laws, then $\boldsymbol{\mathcal{W}}^{\mathrm{T}} = \partial \mathcal{S}/\partial \boldsymbol{\mathcal{U}}$ symmetrizes them.*

Proof. The proof of this theorem can be found in references [39,40]. □

Contracting the Cartesian form of the Euler equations (3) with the entropy variables, $\boldsymbol{\mathcal{W}}$, results in a new scalar differential equation for the entropy,

$$\boldsymbol{\mathcal{W}}^{\mathrm{T}}\frac{\partial \boldsymbol{\mathcal{U}}}{\partial t} + \boldsymbol{\mathcal{W}}^{\mathrm{T}}\sum_{m=1}^{3}\frac{\partial \boldsymbol{\mathcal{F}}_m}{\partial x_m} = \frac{\partial \mathcal{S}}{\partial t} + \sum_{m=1}^{3}\frac{\partial \mathcal{F}_m}{\partial x_m} = 0. \tag{8}$$

Integrating (8) over the domain, Ω, results in a global conservation statement on the entropy in the domain,

$$\frac{\mathrm{d}}{\mathrm{d}t}\int_{\Omega} \mathcal{S}\mathrm{d}\Omega + \oint_{\Gamma}\sum_{m=1}^{3}\mathcal{F}_m n_{x_m}\mathrm{d}\Gamma = 0, \tag{9}$$

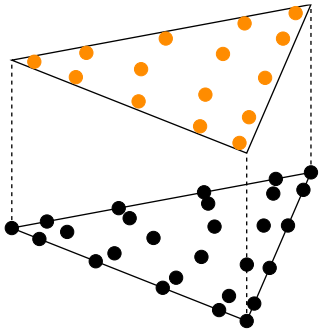

Fig. 2. Staggered grid: ● solution nodes ● flux nodes.

which demonstrates that the entropy can only change in the domain based on the data that convects through the boundaries of Γ.

The integral statement of entropy conservation (9) is not strictly valid in the presence of discontinuities, e.g., shocks, and does not account for the dissipation of the entropy at the discontinuity. While the exact amount of entropy dissipated at a discontinuity is not known a priori, what is known is the sign of the jump in entropy. Thus, it is possible to construct a general but not sharp statement of the global behavior of the entropy in the entire domain as

$$\frac{\mathrm{d}}{\mathrm{d}t}\int_{\Omega} \mathcal{S}\mathrm{d}\Omega + \oint_{\Gamma} \sum_{m=1}^{3} \mathcal{F}_m n_{x_m}\mathrm{d}\Gamma \leq 0.$$

Remark 4. A sufficient condition to ensure the convexity of the entropy function $\mathcal{S} = \mathcal{S}(\mathcal{U})$ and, therefore, a one-to-one mapping between the entropy variables, $\boldsymbol{\mathcal{V}}$, and the conservative variables, $\boldsymbol{\mathcal{U}}$, is that $\rho, T > 0$ (for the proof see for example, Appendix B.1 in reference [20]). Thus,

$$\boldsymbol{\mathcal{V}}^{\mathrm{T}} \frac{\partial^2 \mathcal{S}}{\partial \boldsymbol{\mathcal{U}}^2} \boldsymbol{\mathcal{V}} > 0, \quad \forall\, \boldsymbol{\mathcal{V}} \neq \mathbf{0}, \quad \rho, T > 0.$$

This (physical and mathematical) restriction on density, ρ, and temperature, T, weakens the entropy proof, making it less than a full measure of nonlinear stability. Another mechanism must be employed to bound ρ and T away from zero to guarantee positivity; positivity preservation will not be considered herein.

4. SBP-preserving interpolation operator

4.1. Existence

We are interested in the development of multidimensional SBP schemes with minimal or near minimal DOFs. Such schemes can be advantageous for explicit time marching approaches as they reduce the number of floating point operations. Moreover, they are particularly important in the context of implicit time marching because of the reduced size of the Jacobian matrix. However, for multidimensional SBP schemes, the optimal nodal distributions tend to be interior only nodes and this results in a significant increase in the computational cost of the interelement coupling for entropy-conservative/stable discretizations.

In order to reduce the cost of interelement coupling for interior only nodal distributions, we extend the staggered entropy conservative/stable tensor-product SBP algorithm of Parsani et al. [1] to multidimensional SBP operators. We introduce two set of nodes. The first is the solution set $\widetilde{C}_\kappa = \left\{\tilde{\boldsymbol{\xi}}_i\right\}_{i=1}^{\widetilde{n}_\kappa}$. On this set of nodes, the conservative variables, $\widetilde{\boldsymbol{u}}_\kappa$, are stored and we assume that a norm matrix, $\widetilde{\mathsf{H}}$, of at least degree $2p-1$ exists and that the degree p Vandermonde matrix has full column rank. The second set, $C_\kappa = \left\{\boldsymbol{\xi}_i\right\}_{i=1}^{n_\kappa}$, is where the derivatives of the fluxes are evaluated and we assume an SBP operator of at least degree p exists, see Fig. 2. To construct our discretization, we need to introduce interpolation operators from the solution nodes to the flux nodes, $\mathsf{I}_{\mathrm{S2F}}$, and from the flux nodes back to the solution nodes, $\mathsf{I}_{\mathrm{F2S}}$. For accuracy and stability, we demand that the interpolation be SBP preserving (we aptly call these SBP preserving interpolation operators), that is they satisfy the following conditions [1]:

$$\begin{aligned} &\text{Accuracy: } \mathsf{I}_{\mathrm{S2F}}\widetilde{\mathsf{V}}_p = \mathsf{V}_p, \quad \mathsf{I}_{\mathrm{F2S}}\mathsf{V}_{\hat{p}}, = \widetilde{\mathsf{V}}_{\hat{p}}, \quad \hat{p} \geq p-1 \\ &\text{Stability: } \widetilde{\mathsf{H}}\mathsf{I}_{\mathrm{F2S}}\mathsf{H}^{-1} = \mathsf{I}_{\mathrm{S2F}}^{\mathrm{T}}. \end{aligned} \tag{10}$$

The interpolation from the flux nodes to the solution nodes need only be degree $p-1$ because it acts on the derivative and so the combination $\mathsf{I}_{F2S}\mathsf{D}$ is of degree p. In (10), we used the degree p Vandermonde matrices $\widetilde{\mathsf{V}}_p$ and V_p on the solution and flux nodes, respectively (see Definition 4).

We now discuss one of the main contributions of this paper. The entropy conservation proofs presented later rely on the existence of the interpolation operators I_{S2F} and I_{F2S} that satisfy (10). To this end, we now present a general theorem on the conditions required for existence of such operators.

Theorem 3. *Interpolation operators that satisfy (10), under conditions to be specified shortly, can be in general constructed as,*

$$\begin{aligned} \mathsf{I}_{S2F} &= \left[\mathsf{V}_p, \mathsf{W}\right]\left[\widetilde{\mathsf{V}}_p, \widetilde{\mathsf{W}}\right]^{-1}, \\ \mathsf{I}_{F2S} &= \widetilde{\mathsf{H}}^{-1}\mathsf{I}_{S2F}^{\mathrm{T}}\mathsf{H}, \end{aligned} \tag{11}$$

where $\widetilde{\mathsf{V}}_p$ and V_p are the degree p Vandermonde matrices, of full column rank, on the solution and flux nodes of size $\widetilde{n}_\kappa \times n_p$ and $n_\kappa \times n_p$, respectively, where $n_p = \binom{p+d}{d}$ (where $\left[\mathsf{V}_p, \mathsf{W}\right]\left[\widetilde{\mathsf{V}}_p, \widetilde{\mathsf{W}}\right]^{-1}$ is to be understood as the multiplication of matrix $\left[\mathsf{V}_p, \mathsf{W}\right]$ against the matrix $\left[\widetilde{\mathsf{V}}_p, \widetilde{\mathsf{W}}\right]^{-1}$). Furthermore, $\widetilde{\mathsf{W}}$ is of size $\widetilde{n}_\kappa \times (\widetilde{n}_\kappa - n_p)$ and is chosen so that $[\widetilde{\mathsf{V}}_p, \widetilde{\mathsf{W}}]$ is invertible. The conditions that must be satisfied so that (11) satisfies (10) are

$$\begin{bmatrix} \mathsf{V}_p^{\mathrm{T}}\mathsf{H}\mathsf{V}_{p-1} & \mathsf{V}_p^{\mathrm{T}}\mathsf{H}\mathsf{X} \\ \mathsf{W}^{\mathrm{T}}\mathsf{H}\mathsf{V}_{p-1} & \mathsf{W}^{\mathrm{T}}\mathsf{H}\mathsf{X} \end{bmatrix} = \begin{bmatrix} \widetilde{\mathsf{V}}_p^{\mathrm{T}}\widetilde{\mathsf{H}}\widetilde{\mathsf{V}}_{p-1} & \widetilde{\mathsf{V}}_p^{\mathrm{T}}\widetilde{\mathsf{H}}\widetilde{\mathsf{X}} \\ \widetilde{\mathsf{W}}^{\mathrm{T}}\widetilde{\mathsf{H}}\widetilde{\mathsf{V}}_{p-1} & \widetilde{\mathsf{W}}^{\mathrm{T}}\widetilde{\mathsf{H}}\widetilde{\mathsf{X}} \end{bmatrix}, \tag{12}$$

where the matrices, W, X, and $\widetilde{\mathsf{X}}$ hold free parameters and are of size $n_\kappa \times (\widetilde{n}_\kappa - n_p)$, $n_\kappa \times (n_\kappa - n_p + 1)$, and $\widetilde{n}_\kappa \times (\widetilde{n}_\kappa - n_p + 1)$, respectively (where for simplicity, we have taken $\hat{p} = p - 1$).

If $\mathsf{V}_p^{\mathrm{T}}\mathsf{H}\mathsf{V}_{p-1} = \widetilde{\mathsf{V}}_p^{\mathrm{T}}\widetilde{\mathsf{H}}\widetilde{\mathsf{V}}_{p-1}$, then one possible choice is to set

$$\widetilde{\mathsf{X}} = 0, \quad \mathsf{X} = 0, \quad \mathsf{W} = \left[\widetilde{\mathsf{W}}^{\mathrm{T}}\widetilde{\mathsf{H}}\widetilde{\mathsf{V}}_{p-1}\left(\mathsf{V}_p^{\mathrm{T}}\mathsf{V}_p\right)^{-1}\mathsf{V}_p^{\mathrm{T}}\mathsf{H}^{-1}\right]^{\mathrm{T}}.$$

Proof. The proof is given in Appendix D. □

The importance of Theorem 3 is that it allows us to construct a simple set of sufficient conditions for the existence of the necessary interpolation operators (see the next corollary). How we construct the interpolation operators, i.e., specifying W and $\widetilde{\mathsf{W}}$, is discussed in Section 4.2.

A consequence of Theorem 3 is

Corollary 1. *If the solution and flux nodes come equipped with at least degree $2p-1$ cubature rules, where both nodal distributions support degree p Vandermonde matrices with full column rank, then SBP preserving interpolation operators exist.*

Additionally, we have

Corollary 2. *Assume that the number of solution nodes is of minimum size, that is $\widetilde{n}_\kappa = \binom{p+d}{d}$ where d is the dimension of the problem, and a norm matrix, $\widetilde{\mathsf{H}}$, of at least degree $2p$ can be found on the solution nodes. Furthermore, assume that a set of flux nodes can be found with a norm matrix, H, of at least degree $2p$, then interpolation operators that satisfy (10) can be constructed as*

$$\mathsf{I}_{S2F} = \mathsf{V}_p\widetilde{\mathsf{V}}_p^{-1}, \quad \mathsf{I}_{F2S} = \widetilde{\mathsf{H}}^{-1}\mathsf{I}_{S2F}^{\mathrm{T}}\mathsf{H}.$$

Moreover, they satisfy the property

$$\mathsf{I}_{F2S}\mathsf{I}_{S2F} = \mathsf{I}, \tag{13}$$

where I is an $\widetilde{n}_\kappa \times \widetilde{n}_\kappa$ identity matrix.

Proof. The proof is given in Appendix E. □

4.2. Construction of the SBP preserving interpolation operators

In this subsection, we give a sketch of our procedure, based on Theorem 3 and its proof, to construct the interpolation operators:

- We use a full rank QR decomposition of $\widetilde{\mathsf{V}}_p$ to construct an orthogonal basis for the null space of $\left(\widetilde{\mathsf{V}}_p\right)^{\mathrm{T}}$ and use this null space to populate $\widetilde{\mathsf{W}}$. That is

$$\widetilde{\mathsf{V}}_p = \mathsf{QR} = [\mathsf{Q}_1, \mathsf{Q}_2] \begin{bmatrix} \mathsf{R}_1 \\ 0 \end{bmatrix} = \mathsf{Q}_1 \mathsf{R}_1,$$

  $\widetilde{\mathsf{W}} = \mathsf{Q}_2$.
- We set $\mathsf{W} = \left[\widetilde{\mathsf{W}}^{\mathrm{T}} \widetilde{\mathsf{H}} \widetilde{\mathsf{V}}_{p-1} \left(\mathsf{V}_p^{\mathrm{T}} \mathsf{V}_p\right)^{-1} \mathsf{V}_p^{\mathrm{T}} \mathsf{H}^{-1}\right]^{\mathrm{T}}$.
- The interpolation operators are constructed as $\mathsf{I}_{\mathrm{S2F}} = \left[\mathsf{V}_p, \mathsf{W}\right] \left[\widetilde{\mathsf{V}}_p, \widetilde{\mathsf{W}}\right]^{-1}, \quad \mathsf{I}_{\mathrm{F2S}} = \widetilde{\mathsf{H}}^{-1} \mathsf{I}_{\mathrm{S2F}}^{\mathrm{T}} \mathsf{H}$.

To make clear why we call these matrices SBP preserving, we note that using these matrices, we have constructed an SBP operator on the solution nodes using an SBP operator on the flux nodes; that is

$$\widetilde{\mathsf{D}}_{\xi_l} \equiv \mathsf{I}_{\mathrm{F2S}} \mathsf{D}_{\xi_l} \mathsf{I}_{\mathrm{S2F}},$$

where using the SBP preserving property we can identify the constituent matrices of the resulting SBP operator as

$$\widetilde{\mathsf{H}}, \qquad \widetilde{\mathsf{Q}}_{\xi_l} \equiv \mathsf{I}_{\mathrm{S2F}}^{\mathrm{T}} \mathsf{Q}_{\xi_l} \mathsf{I}_{\mathrm{S2F}}, \qquad \widetilde{\mathsf{S}}_{\xi_l} \equiv \mathsf{I}_{\mathrm{S2F}}^{\mathrm{T}} \mathsf{S}_{\xi_l} \mathsf{I}_{\mathrm{S2F}}, \qquad \widetilde{\mathsf{E}}_{\xi_l} \equiv \mathsf{I}_{\mathrm{S2F}}^{\mathrm{T}} \mathsf{E}_{\xi_l} \mathsf{I}_{\mathrm{S2F}}.$$

5. Staggered-grid discretization of the Euler equations

We need to present some additional mechanics before introducing our entropy conservative discretization of the Euler equations. Specifically, we introduce dyadic flux functions with specific properties. Let $\boldsymbol{\mathcal{F}}_m^{\star}(\cdot,\cdot) : \mathbb{R}^5 \times \mathbb{R}^5 \to \mathbb{R}^5$ denote a numerical flux function with the following properties

$$\begin{aligned} &\text{Symmetry: } \boldsymbol{\mathcal{F}}_m^{\star}\left(\boldsymbol{\mathcal{U}}, \boldsymbol{\mathcal{U}}'\right) = \boldsymbol{\mathcal{F}}_m^{\star}\left(\boldsymbol{\mathcal{U}}', \boldsymbol{\mathcal{U}}\right), \\ &\text{Consistency: } \boldsymbol{\mathcal{F}}_m^{\star}\left(\boldsymbol{\mathcal{U}}, \boldsymbol{\mathcal{U}}\right) = \boldsymbol{\mathcal{F}}_m, \\ &\text{Tadmor shuffle: } \left(\boldsymbol{\mathcal{W}} - \boldsymbol{\mathcal{W}}'\right)^{\mathrm{T}} \boldsymbol{\mathcal{F}}_m^{\star}\left(\boldsymbol{\mathcal{U}}, \boldsymbol{\mathcal{U}}'\right) = \Psi_m - \Psi_m'. \end{aligned} \tag{14}$$

A flux that satisfies the above conditions was first presented by Tadmor [14]. Subsequently, Ismail and Roe [41] and Chandrashekar [42] developed less expensive numerical fluxes that satisfy the same conditions. In this paper, we use the Ismail-Roe flux with the log-avg accuracy improvement suggested in [21].

The solution vector $\widetilde{\boldsymbol{u}}_\kappa \in \mathbb{R}^{5\widetilde{n}_\kappa}$ on the κth element is organized as

$$\widetilde{\boldsymbol{u}}_{\kappa,i} \equiv \widetilde{\boldsymbol{u}}_\kappa(5(i-1)+1:5i) = \left[\mathcal{U}_1(\widetilde{\boldsymbol{\xi}}_i), \mathcal{U}_2(\widetilde{\boldsymbol{\xi}}_i), \mathcal{U}_3(\widetilde{\boldsymbol{\xi}}_i), \mathcal{U}_4(\widetilde{\boldsymbol{\xi}}_i), \mathcal{U}_5(\widetilde{\boldsymbol{\xi}}_i)\right]^{\mathrm{T}},$$

where we recollect that the subscript i denotes the local node number. In addition, we will need to refer to vectors of the components of the solution vector over the element and use the notation $\widetilde{\boldsymbol{u}}_\kappa^{(i)}$. For example, $\widetilde{\boldsymbol{u}}_\kappa^{(1)}$ denotes the density at the nodes of element κ.

We now present the entropy conservative discretization of the skew-symmetric form of the Euler equations (4), i.e., which is a splitting based on the metric terms:

$$\frac{\mathrm{d}\overline{\widetilde{\mathsf{J}}}_\kappa \widetilde{\boldsymbol{u}}_\kappa}{\mathrm{d}t} + \overline{\mathsf{I}}_{\mathrm{F2S}} \sum_{l,m=1}^{3} \left[\left(\overline{\mathsf{D}}_{\xi_l} \overline{\mathsf{A}}_\kappa^{l,m} + \overline{\mathsf{A}}_\kappa^{l,m} \overline{\mathsf{D}}_{\xi_l}\right) \circ \mathsf{F}_m(\boldsymbol{u}_\kappa, \boldsymbol{u}_\kappa)\right] \overline{\mathbf{1}} = \boldsymbol{SAT}, \tag{15}$$

with

$$\begin{aligned} &\boldsymbol{SAT} \equiv \overline{\mathsf{I}}_{\mathrm{F2S}} \overline{\mathsf{H}}^{-1} \sum_{l,m=1}^{3} \left(\overline{\mathsf{E}}_{\xi_l} \overline{\mathsf{A}}_\kappa^{l,m}\right) \circ \mathsf{F}_m(\boldsymbol{u}_\kappa, \boldsymbol{u}_\kappa) \overline{\mathbf{1}} - \overline{\mathsf{I}}_{\mathrm{F2S}} \overline{\mathsf{H}}^{-1} \sum_{\gamma \subset \partial\hat{\Omega}_\kappa} \sum_{l,m=1}^{3} \overline{\mathsf{E}}_{\xi_l,m,\gamma}^{\kappa,\nu} \circ \mathsf{F}_m(\boldsymbol{u}_\kappa, \boldsymbol{u}_\nu) \overline{\mathbf{1}}, \\ &\overline{\mathsf{H}} \equiv \mathsf{H} \otimes \mathsf{I}_5, \qquad \overline{\widetilde{\mathsf{H}}} \equiv \widetilde{\mathsf{H}} \otimes \mathsf{I}_5, \qquad \overline{\mathsf{D}}_{\xi_l} \equiv \mathsf{D}_{\xi_l} \otimes \mathsf{I}_5, \qquad \overline{\mathsf{Q}}_{\xi_l} \equiv \mathsf{Q}_{\xi_l} \otimes \mathsf{I}_5, \qquad \overline{\mathsf{E}}_{\xi_l} \equiv \mathsf{E}_{\xi_l} \otimes \mathsf{I}_5, \\ &\overline{\mathsf{E}}_{\xi_l,m,\gamma}^{\kappa,\nu} \equiv \mathsf{E}_{\xi_l,m,\gamma}^{\kappa,\nu} \otimes \mathsf{I}_5, \qquad \overline{\widetilde{\mathsf{J}}}_\kappa \equiv \widetilde{\mathsf{J}}_\kappa \otimes \mathsf{I}_5, \qquad \overline{\mathsf{A}}_\kappa^{l,m} = \mathsf{A}_\kappa^{l,m} \otimes \mathsf{I}_5, \quad \overline{\mathbf{1}} \equiv \mathbf{1} \otimes \mathbf{1}_5, \quad \overline{\mathsf{I}}_{\mathrm{F2S}} \equiv \mathsf{I}_{\mathrm{F2S}} \otimes \mathsf{I}_5, \end{aligned}$$

where I_5 is a 5×5 identity matrix, $\mathbf{1}_5$ is a vectors of ones with 5 entries, and the notation, for example, $\mathbf{1}$ denotes a vector of ones having n_κ entries. Furthermore, the diagonal matrices, $\widetilde{\mathsf{J}}_\kappa$ and $\mathsf{A}_\kappa^{l,m}$ are constructed from approximations to the analytical metric Jacobian and metric terms, respectively, and are given as

$$\widetilde{\mathsf{J}}_\kappa \approx \mathrm{diag}\left[\mathcal{J}_\kappa(\widetilde{\boldsymbol{\xi}}_1), \ldots, \mathcal{J}_\kappa(\widetilde{\boldsymbol{\xi}}_{n_\kappa})\right], \qquad \mathsf{A}_\kappa^{l,m} \approx \mathrm{diag}\left[\mathcal{A}_\kappa^{l,m}(\boldsymbol{\xi}_1), \ldots, \mathcal{A}_\kappa^{l,m}(\boldsymbol{\xi}_{n_\kappa})\right].$$

Remark 5. In Appendix A we discuss how (15) can be recast such that we reduce floating point operations at the cost of memory.

The matrices $\mathsf{F}_m(\boldsymbol{u}_\kappa, \boldsymbol{u}_\nu) \in \mathbb{R}^{5n_\kappa \times 5n_\nu}$ are defined by

$$\mathsf{F}_m(\boldsymbol{u}_\kappa, \boldsymbol{u}_\nu) \equiv \begin{bmatrix} \operatorname{diag}\left[\boldsymbol{\mathcal{F}}_m^\star\left(\boldsymbol{u}_{\kappa,1}, \boldsymbol{u}_{\nu,1}\right)\right] & \dots & \operatorname{diag}\left[\boldsymbol{\mathcal{F}}_m^\star\left(\boldsymbol{u}_{\kappa,1}, \boldsymbol{u}_{\nu,n_\nu}\right)\right] \\ \vdots & \ddots & \vdots \\ \operatorname{diag}\left[\boldsymbol{\mathcal{F}}_m^\star\left(\boldsymbol{u}_{\kappa,n_\kappa}, \boldsymbol{u}_{\nu,1}\right)\right] & \dots & \operatorname{diag}\left[\boldsymbol{\mathcal{F}}_m^\star\left(\boldsymbol{u}_{\kappa,n_\kappa}, \boldsymbol{u}_{\nu,n_\nu}\right)\right] \end{bmatrix}.$$

It follows from the symmetry of $\boldsymbol{\mathcal{F}}_m^\star$ that F_m has the property

$$\mathsf{F}_m(\boldsymbol{u}_\kappa, \boldsymbol{u}_\nu) = \mathsf{F}_m(\boldsymbol{u}_\nu, \boldsymbol{u}_\kappa)^{\mathrm{T}}.$$

Similarly, we have a scalar version given as

$$\mathsf{F}_m^{(i)}(\boldsymbol{u}_\kappa, \boldsymbol{u}_\nu) \equiv \begin{bmatrix} \boldsymbol{\mathcal{F}}_m^\star\left(\boldsymbol{u}_{\kappa,1}, \boldsymbol{u}_{\nu,1}\right)(i) & \dots & \boldsymbol{\mathcal{F}}_m^\star\left(\boldsymbol{u}_{\kappa,1}, \boldsymbol{u}_{\nu,n_\nu}\right)(i) \\ \vdots & \ddots & \vdots \\ \boldsymbol{\mathcal{F}}_m^\star\left(\boldsymbol{u}_{\kappa,n_\kappa}, \boldsymbol{u}_{\nu,1}\right)(i) & \dots & \boldsymbol{\mathcal{F}}_m^\star\left(\boldsymbol{u}_{\kappa,n_\kappa}, \boldsymbol{u}_{\nu,n_\nu}\right)(i) \end{bmatrix}, \quad i = 1, 2, \dots, 5.$$

The semidiscrete entropy analysis relies on the Tadmor-shuffle condition and in order for the staggered discretization to retain this property, the arguments of the F_m entries have to be constructed as

$$\boldsymbol{u}_\kappa \equiv \boldsymbol{\mathcal{U}}\left(\mathsf{I}_{\mathrm{S2F}}\tilde{\boldsymbol{w}}_\kappa\right), \qquad \boldsymbol{u}_\nu \equiv \boldsymbol{\mathcal{U}}\left(\mathsf{I}_{\mathrm{S2F}}\tilde{\boldsymbol{w}}_\nu\right).$$

We now present some accuracy estimates for the components of the discretization that follow directly from the work in [4,43]. For the nonlinear differentiation operators, we have the following theorem:

Theorem 4. *Let $\overline{\mathsf{D}}_{\xi_l}$ be a degree p differentiation matrix that approximates the first derivative $\frac{\partial}{\partial \xi_l}$, on a set of nodes C_κ. Consider a PDE whose fluxes in the x_m coordinate directions, $m = 1, 2, 3$, are continuously differentiable functions $\boldsymbol{\mathcal{F}}_{\kappa,m} : \mathcal{R}^5 \to \mathcal{R}^5$. In addition, consider metric terms $\mathcal{A}_\kappa^{l,m}$ that satisfy the metric identities (5) and are sufficiently smooth. If the two-point flux function $\boldsymbol{\mathcal{F}}_m^\star$ is continuously differentiable, consistent, and symmetric, then for sufficiently smooth $\boldsymbol{\mathcal{U}}$*

$$\begin{aligned} \sum_{l=1}^{3}\left[\bar{\mathsf{I}}_{\mathrm{F2S}}\left(2\overline{\mathsf{D}}_{\xi_l}\overline{\mathsf{A}}_\kappa^{l,m} \circ \mathsf{F}_m\left(\boldsymbol{\mathcal{U}}, \boldsymbol{\mathcal{U}}\right)\right)\overline{\mathbf{1}}\right] &= \sum_{l=1}^{3}\frac{\partial}{\partial \xi_l}\left(\mathcal{A}_\kappa^{l,m}\boldsymbol{\mathcal{F}}_m\right)\Big|_{C_\kappa} + \mathcal{O}\left(h^{p+d}\right), \\ \left[\bar{\mathsf{I}}_{\mathrm{F2S}}\overline{\mathsf{A}}_\kappa^{l,m}\left(2\overline{\mathsf{D}}_{\xi_l} \circ \mathsf{F}_m\left(\boldsymbol{\mathcal{U}}, \boldsymbol{\mathcal{U}}\right)\right)\overline{\mathbf{1}}\right] &= \mathcal{A}_\kappa^{l,m}\frac{\partial \boldsymbol{\mathcal{F}}_m}{\partial \xi_l}\Big|_{C_\kappa} + \mathcal{O}\left(h^{p+d}\right), \end{aligned} \tag{16}$$

where h is some appropriate measure of the mesh spacing within the element.

Proof. The proof follows from REFs. [4,43] and the accuracy properties of the interpolation operator $\mathsf{I}_{\mathrm{F2S}}$. We note that in the first estimate, we have taken advantage of the metric identities since for a general variable coefficient $\mathcal{A}$

$$\left[\bar{\mathsf{I}}_{\mathrm{F2S}}\left(2\overline{\mathsf{D}}_{\xi_l}\overline{\mathsf{A}} \circ \mathsf{F}_m\left(\boldsymbol{\mathcal{U}}, \boldsymbol{\mathcal{U}}\right)\right)\overline{\mathbf{1}}\right] = \left[\frac{\partial}{\partial \xi_l}\left(\mathcal{A}\boldsymbol{\mathcal{F}}_m\right) + \boldsymbol{\mathcal{F}}_m\frac{\partial \mathcal{A}}{\partial \xi_l}\right]\Big|_{C_\kappa} + \mathcal{O}\left(h^{p+1}\right).$$

We also note that the d in estimate (16) comes from the fact that in transforming to curvilinear coordinates, we have multiplied the PDE by $\mathcal{J}$, which is of order $\mathcal{O}\left(h^d\right)$ and similarly, the metric terms, $\mathcal{A}_\kappa^{l,m}$, are of order $\mathcal{O}\left(h^{d-1}\right)$. □

For the coupling SAT, we have the following theorem:

Theorem 5. *Under the same conditions as in Theorem 4, the **SAT** penalty in (15) satisfies*

$$\boldsymbol{SAT} = \mathcal{O}(h^{r+d}),$$

where $r \geq p$ is the constant that appears in Definition 3.

Proof. See Thrm. 2 Crean et al. [4] (our estimate here differs by d for the previously mentioned reason). □

As a result of Thrms. 4 and 5, we see that all components of the discretization are at least degree p. In proving elementwise conservation, we require the following theorem concerning the accuracy of the coupling matrices in the SAT (in a weak sense):

Theorem 6. *The coupling matrices are approximations to the following surface integrals:*

$$\boldsymbol{v}_\kappa^{\mathrm{T}}\left[\mathsf{E}^{\kappa,\nu}_{\xi_l,m,\gamma}\circ\mathsf{F}^{(i)}_m\left(\boldsymbol{u}_\kappa,\boldsymbol{u}_\nu\right)\mathbf{1}\right]=\oint_\gamma \mathcal{V}\boldsymbol{\mathcal{F}}_{x_m}(i)\mathcal{J}_\kappa\frac{\partial\xi_l}{\partial x_m}n_{\xi_l}\mathrm{d}\hat{\Gamma}+\mathcal{O}\left(h^{r+d}\right),\qquad l=1,2,3,\qquad i=1,\ldots,5.$$

Proof. The proof is given in Del Rey Fernández et al. [43]. □

5.1. Semidiscrete entropy conservation

The purpose of the nonlinear SBP differentiation matrix (and coupling mechanics) introduced in the previous section is to construct a scheme on which we can perform a semidiscrete entropy stability analysis that is related to the continuous analysis in a one-to-one fashion.

Our starting point is to construct an entropy conservative scheme (we prove entropy conservation in this section) and then add appropriate dissipation (discussed in Section 5.3) in order to achieve entropy stability. To prove entropy conservation, we introduce the following lemma [43]:

Lemma 1. *Consider the matrix* A *of size* $n\times n'$. *If the two argument matrix flux function* $\mathsf{F}\left(\boldsymbol{u},\boldsymbol{u}'\right)$ *is built using a two point flux function that is symmetric in its arguments and satisfies the Tadmor shuffle condition, then*

$$\boldsymbol{w}^{\mathrm{T}}\left(\mathsf{A}\otimes\mathsf{I}_5\right)\circ\mathsf{F}\left(\boldsymbol{u},\boldsymbol{u}'\right)\overline{\mathbf{1}}'-\overline{\mathbf{1}}^{\mathrm{T}}\left(\mathsf{A}\otimes\mathsf{I}_5\right)\circ\mathsf{F}\left(\boldsymbol{u}',\boldsymbol{u}\right)\boldsymbol{w}'=\boldsymbol{\psi}^{\mathrm{T}}\left(\mathsf{A}\otimes\mathsf{I}_5\right)\mathbf{1}_r-\left(\mathbf{1}'\right)^{\mathrm{T}}\left(\mathsf{A}\otimes\mathsf{I}_5\right)\boldsymbol{\psi}'.$$

We can now prove the following theorem:

Theorem 7. *Discretization* (15) *is discretely entropy conservative, that is, e.g., for the periodic problem we have that*

$$\sum_{\kappa=1}^{K}\widetilde{\widetilde{\mathbf{1}}}^{\mathrm{T}}\widetilde{\widetilde{\mathsf{J}}}_\kappa\widetilde{\widetilde{\mathsf{H}}}\frac{\mathrm{d}\widetilde{\boldsymbol{s}}_\kappa}{\mathrm{d}t}=0,$$

if the metric terms, $\mathsf{A}^{l,m}_\kappa$, *are constructed such that*

$$\sum_{m=1}^{3}\mathsf{D}_{\xi_l}\mathsf{A}^{l,m}_\kappa\mathbf{1}=\mathsf{H}^{-1}\left(\sum_{m=1}^{3}\mathsf{E}_{\xi_l}\mathsf{A}^{l,m}_\kappa\mathbf{1}-\sum_{\gamma\subset\partial\hat{\Omega}_k}\sum_{l,m=1}^{3}\mathsf{E}^{\kappa,\nu}_{\xi_l,m,\gamma}\mathbf{1}\right),\tag{17}$$

and the interpolation operators satisfy the stability condition

$$\widetilde{\mathsf{H}}\mathsf{I}_{\mathrm{F2S}}\mathsf{H}^{-1}=\mathsf{I}^{\mathrm{T}}_{\mathrm{S2F}}.\tag{18}$$

Proof. The proof is given in Appendix B. □

We use the approach of Crean et al. [4] to approximate the metrics such that (17) is satisfied. The basic idea is to solve a convex optimization problem such that we satisfy (17) and are optimally close, in the Cartesian norm, to the analytical metrics (in Crean et al. [4] it is proven that the rate of convergence of the metric terms is $\mathcal{O}\left(h^{p+2}\right)$). For two-dimensional problems, if the curvilinear coordinate transformation is of degree $\leq p+1$ then the equation (17) is satisfied automatically because the metric terms are of degree $\leq p$ and therefore, the various operators involved in (17) are exact (see Crean et al. [4]).

5.2. Elementwise conservation

The nonlinear hyperbolic nature of the Euler equations (4) means that in finite time, nonsmooth solutions can result despite being closed with smooth data; therefore, in such cases, it is necessary to consider the integral form of the conservation law or the space-time weak form. In this paper, we consider the weak form, which is given as

$$\int_{t=0}^{T}\int_{\hat{\Omega}_\kappa}\boldsymbol{\mathcal{U}}\frac{\partial\mathcal{V}}{\partial t}+\sum_{l,m=1}^{3}\mathcal{A}^{l,m}\boldsymbol{\mathcal{F}}_m\frac{\partial\mathcal{V}}{\partial\xi_l}\mathrm{d}\hat{\Omega}\mathrm{d}t-\int_{\hat{\Omega}_\kappa}\mathcal{V}\boldsymbol{\mathcal{U}}\big|_{t=0}^{T}\mathrm{d}\hat{\Omega}-\int_{t=0}^{T}\oint_{\hat{\Gamma}_\kappa}\sum_{l,m=1}^{3}\mathcal{A}^{l,m}\boldsymbol{\mathcal{F}}_m n_{\xi_l}\mathrm{d}\hat{\Gamma}\mathrm{d}t=\mathbf{0},\tag{19}$$
$$t>0,\qquad\kappa=1,\ldots,K,$$

for all smooth test functions $\mathcal{V}$ with compact support.

The integral and weak forms are equivalent and both support a restricted class of discontinuous solutions that satisfy the jump conditions

$$s[[\mathcal{U}]] = [[\mathcal{F}]],$$

where s is the speed of the discontinuity and $[[\mathcal{U}]]$ is the jump in $\mathcal{U}$ across the discontinuity. Our interest is in numerically approximating this restricted set of discontinuous solutions that satisfy the above jump conditions — for example, in the case of the Euler equations these are known as the Rankine-Hugoniot jump conditions. Thus, the class of schemes that we are interested in are those that are consistent approximations of (19). In this paper, we take a method of lines approach; thus, rather than (19), we discuss conservation in the context of

$$\int_{\hat{\Omega}_\kappa} \mathcal{V}\frac{\partial \mathcal{U}}{\partial t}\mathcal{J}_\kappa \mathrm{d}\hat{\Omega} - \int_{\hat{\Omega}_\kappa} \sum_{l,m=1}^{3} \mathcal{A}_\kappa^{l,m}\mathcal{F}_m \frac{\partial \mathcal{V}}{\partial \xi_l}\mathrm{d}\hat{\Omega} + \oint_{\hat{\Gamma}_\kappa} \mathcal{V}\mathcal{A}_\kappa^{l,m}\mathcal{F}_m n_{\xi_l}\mathrm{d}\hat{\Gamma} = 0, \quad \kappa = 1,\ldots,K. \tag{20}$$

Conservation of the fully discrete scheme can always be achieved with an appropriate choice of time integration scheme.

Our proof of elementwise conservation is based on the extension of the Lax-Wendroff Thrm. recently proposed by Shi and Shu [44] and subsequently used by Del Rey Fernández et al. [43]. The essential idea is to recast the discretization in a telescoping form; e.g., in one dimension, we obtain a finite-volume-like scheme

$$\frac{\mathrm{d}\overline{\boldsymbol{u}}_\kappa}{\mathrm{d}t} + \boldsymbol{g}^\kappa_{j+1/2} - \boldsymbol{g}^\kappa_{j-1/2} = \boldsymbol{0},$$

where $\overline{\boldsymbol{u}}_\kappa$ is a generalized locally conserved quantity and the $\boldsymbol{g}$'s are unique generalized surface fluxes. In the multidimensional version, we need to show that our semidiscrete equations satisfy the following:

- Telescoping form: Our scheme can be algebraically manipulated into telescoping flux form at the element level generically given as

$$\frac{\mathrm{d}\overline{\boldsymbol{u}}_\kappa}{\mathrm{d}t} + \sum_{\gamma\subset\partial\hat{\Omega}_\kappa} \boldsymbol{g}^\kappa_\gamma = \boldsymbol{0}. \tag{21}$$

- Consistency: Given a constant flow $\mathcal{U} = \mathcal{U}_c$,

$$\begin{aligned} \overline{\boldsymbol{u}}_\kappa &= \left(\int_{\hat{\Omega}_\kappa} \mathcal{J}_\kappa \mathrm{d}\hat{\Omega} + \mathcal{O}(h)\right)\mathcal{U}_c, \\ \boldsymbol{g}^\kappa_\gamma &= \sum_{l,m=1}^{3}\left[\oint_\gamma \mathcal{J}_\kappa \mathcal{A}_\kappa^{l,m} n_{\xi_l}\mathrm{d}\hat{\Gamma} + \mathcal{O}(h)\right]\mathcal{F}_m. \end{aligned} \tag{22}$$

- Boundedness: The generalized conserved quantity and fluxes are bounded in terms of the L^∞ norm of the numerical solution:

$$\begin{aligned} &\left|\overline{\boldsymbol{u}}_k(i) - \overline{\boldsymbol{v}}_\kappa(i)\right| \le C\left\|\boldsymbol{u}^{(i)}_\kappa - \boldsymbol{v}^{(i)}_\kappa\right\|_{L^\infty}, \\ &\left|\left(\boldsymbol{g}^\kappa_\gamma(\boldsymbol{u}_\kappa)\right)(i) - \left(\boldsymbol{g}^\kappa_\gamma(\boldsymbol{v}_\kappa)\right)(i)\right| \le C\left\|\boldsymbol{u}^{(i)}_\kappa - \boldsymbol{v}^{(i)}_\kappa\right\|_{L^\infty}, \end{aligned} \tag{23}$$

  where $\boldsymbol{v}_\kappa$ is another numerical solution and C is some positive constant.
- Global conservation:

$$\sum_{\kappa=1}^{K}\overline{\boldsymbol{u}}_\kappa(i) = \int_\Omega \mathcal{U}(i)\mathrm{d}\Omega + \mathcal{O}(h).$$

Following the work in REF. [43], we have the following result

Theorem 8. *If the coupling matrices, $\overline{\mathrm{E}}^{\kappa,\nu}_{\xi_l,m,\gamma}$, on either side of a given interface are the negative transpose of each other, then the semidiscrete form (15) can be algebraically manipulated into elementwise telescoping form (21) where*

$$\overline{\boldsymbol{u}}_\kappa(i) \equiv \widetilde{\mathbf{1}}^{\mathrm{T}}\widetilde{\mathsf{H}}\widetilde{\mathsf{J}}_\kappa \boldsymbol{u}_\kappa^{(i)},$$
$$\boldsymbol{g}_\gamma^\kappa(i) \equiv \mathbf{1}^{\mathrm{T}} \sum_{l,m=1}^{3} \mathsf{E}^{\kappa,\nu}_{\xi_l,m,\gamma} \circ \mathsf{F}_m^{(i)}(\boldsymbol{u}_\kappa, \boldsymbol{u}_\nu)\mathbf{1}, \quad i = 1, 2, \ldots, 5.$$

If in addition, they satisfy the following consistency conditions, then the scheme is elementwise conservative: for a constant state $\boldsymbol{\mathcal{U}}_c$

$$\mathbf{1}^{\mathrm{T}}\mathsf{E}^{\kappa,\nu}_{\xi_l,m,\gamma} \circ \mathsf{F}_m^{(i)}(\boldsymbol{u}_\kappa, \boldsymbol{u}_\nu)\mathbf{1} = \left[\oint_\gamma \mathcal{J}_\kappa \frac{\partial \xi_l}{\partial x_m} n_{\xi_l} \mathrm{d}\hat{\Gamma}\right] \boldsymbol{\mathcal{F}}_m(i), \quad i = 1, 2, \ldots, 5.$$

Proof. The proof follows directly from the work in REF. [43]; for completeness the proof is included in Appendix C. □

Finally, if the discrete metric identities are satisfied, then the scheme has the free-stream preservation property.

Theorem 9. *The semidiscrete equations preserve the free stream if the discrete metric terms satisfy* (17)*.*

Proof. The proof is identical to that given in REF. [43] and is included in Appendix F for completeness. □

5.3. Entropy stable discretization of the Euler equations

While the entropy conservative scheme gives dissipation free stability, it is physically inconsistent for nonsmooth flows as it violates the second law of thermodynamics and we therefore need to introduce some form of dissipation. In this section, we consider a Lax-Friedrichs like interface dissipation augmentation of the SATs; we follow the work of Crean et al. [4] and add to the right-hand side of (15) the following dissipation terms:

$$\boldsymbol{diss} \equiv -\bar{\mathsf{I}}_{\mathrm{F2S}}\overline{\mathsf{H}}^{-1} \sum_{\gamma\subset\partial\hat{\Omega}_\kappa} \overline{\mathsf{R}}^{\mathrm{T}}_{\gamma\kappa}\Lambda_\gamma \overline{\mathsf{B}}_\gamma \left(\overline{\mathsf{R}}_{\gamma\kappa}\boldsymbol{w}_\kappa - \overline{\mathsf{R}}_{\gamma\nu}\boldsymbol{w}_\nu\right),$$

where $\boldsymbol{w}_\kappa \equiv \mathsf{I}_{\mathrm{S2F}}\tilde{\boldsymbol{w}}_\kappa$ and $\boldsymbol{w}_\nu \equiv \mathsf{I}_{\mathrm{S2F}}\tilde{\boldsymbol{w}}_\nu$. The added terms should be dissipative, design order, and result in an entropy stable and elementwise conservative scheme; this is treated in the next theorem [4].

Theorem 10. *If the matrices* Λ_γ*, are composed of* 5×5 *symmetric semidefinite blocks along the diagonal, then they result in an addition of dissipative terms of order* $\mathcal{O}\left(h_m^r\right)$ *that maintain the elementwise conservation properties of the underlying scheme.*

Proof. The proof follows identically to Thrm. 5 in Crean et al. [4]. □

To construct the Λ matrices, we follow the work of Crean et al. [4] and construct them such that the ith 5×5 block is given by

$$|\lambda_{\max}| \frac{\partial \boldsymbol{\mathcal{U}}}{\partial \boldsymbol{\mathcal{W}}},$$

where $|\lambda_{\max}|$ is an approximation to the magnitude of the fastest wave speed of the flux in the (scaled) normal direction to the interface under consideration. The scaled normal vectors are defined as $\mathsf{N}_x = \sum_{l=1}^{3} \mathsf{A}_\gamma^{l,1}\mathsf{N}_{\xi_l,\gamma}$ in the x direction and similarly in the y direction. The Jacobian of the conserved variables with respect to the entropy variables, i.e., $\frac{\partial \boldsymbol{\mathcal{U}}}{\partial \boldsymbol{\mathcal{W}}}$ is evaluated at the average state of the interpolation/extrapolation of the conserved variables onto the face nodes.

6. Numerical experiments

In this section, we aim to characterize the staggered-grid approach as compared to the collocated approach as well as to verify the theoretical properties of the semidiscrete algorithm.

The SBP operators that we consider are displayed in Figs. 3 and 4. The SBP-Ω operators have interior only solution nodes and dense-E, while the SBP diagonal-E operators have collocated surface cubature nodes. In the numerical experiments, we consider staggering with solution nodes on the Ω nodes and the flux nodes on the diagonal-E nodes for equal p. For all simulations, we use LSERK54 to discretize in time [45].

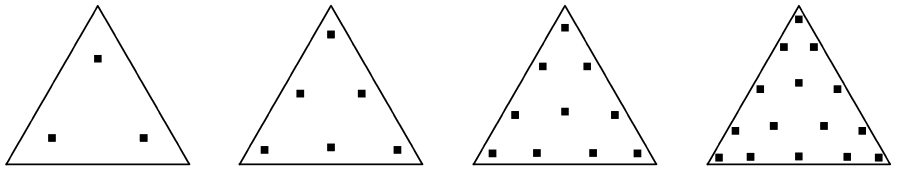

(a) $p = 1$ (b) $p = 2$ (c) $p = 3$ (d) $p = 4$

Fig. 3. SBP-Ω elements.

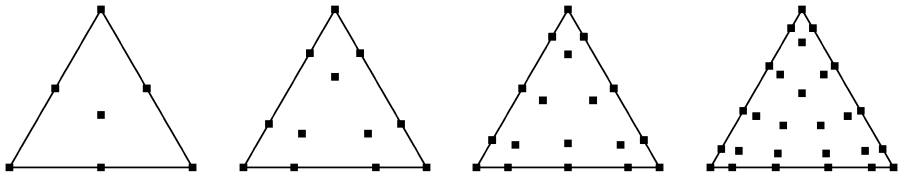

(a) $p = 1$ (b) $p = 2$ (c) $p = 3$ (d) $p = 4$

Fig. 4. SBP Diagonal-E elements.

6.1. Convergence study

To test the accuracy of the algorithm, we solve the isentropic Euler vortex propagation problem. The analytical solution is

$$\begin{aligned} f(x,y,t) &= 1 - \left((x - x_0 - U_\infty \cos(\alpha)t)^2 + (y - y_0 - U_\infty \sin(\alpha)t)^2\right) \\ T(x,y,t) &= 1 - \epsilon^2 M_\infty^2 \frac{\gamma - 1}{8\pi^2} e^{f(x,y,t)} \\ \rho(x,y,t) &= T^{\frac{1}{\gamma - 1}} \\ u(x,y,t) &= U_\infty \cos(\alpha) - \epsilon \frac{y - y_0 - U_\infty \sin(\alpha)t}{2\pi} e^{\frac{f(x,y,t)}{2}} \\ v(x,y,t) &= U_\infty \sin(\alpha) + \epsilon \frac{x - x_0 - U_\infty \sin(\alpha)t}{2\pi} e^{\frac{f(x,y,t)}{2}} \end{aligned} \tag{24}$$

where $U_\infty = 1$, $M_\infty = 0.5$, $\epsilon = 5$, $\alpha = 45$ degrees, and $x_0 = y_0 = 0.0$. For all problems in this paper, $\gamma = 1.4$.

We perform a mesh refinement study with meshes having 4^2 through 256^2 elements, where subsequent meshes are obtained by doubling the number of elements. The domain is a square $(x, y) \in [-5, 5]$ and the curvilinear coordinate transformation is given by

$$\begin{aligned} x_i^* &= \frac{x_i - x_{i,\min}}{x_{i,\max} - x_{\min}} \\ x_i^* &\leftarrow x_i^* + \frac{1}{40}\sin(2\pi x_i^*) \\ x_i &= x_i^*(x_{i,\max} - x_{\min}) + x_{i,\min}, \end{aligned}$$

where $x_{i,\max}$ and $x_{i,\min}$ are the maximum and minimum coordinates in the ith direction. Representative meshes are displayed in Fig. 6.

The CFL is set to 0.25 based on the mesh spacing on the solution grid and is computed via the following formula:

$$h = \frac{h_{\text{node}}}{n} \sum_{i=1}^{n} (\mathcal{J}_i)^{-d},$$

where h_{node} is the minimum distance between nodes on the reference element, $\mathcal{J}_i$ is the determinant of the mapping Jacobian at node i, n is the number of nodes in the mesh, and d is the dimensionality of the equations (either 2 or 3).

The vortex at the start of the simulation is centered and advects at a 45° angle to the upper right; we impose Dirichlet boundary conditions with a standard Roe-type SAT (see [9]). This boundary condition has not been proven to be entropy-stable; however, previous studies such as [46] have shown this boundary condition to be stable when combined with the entropy stable interior scheme.

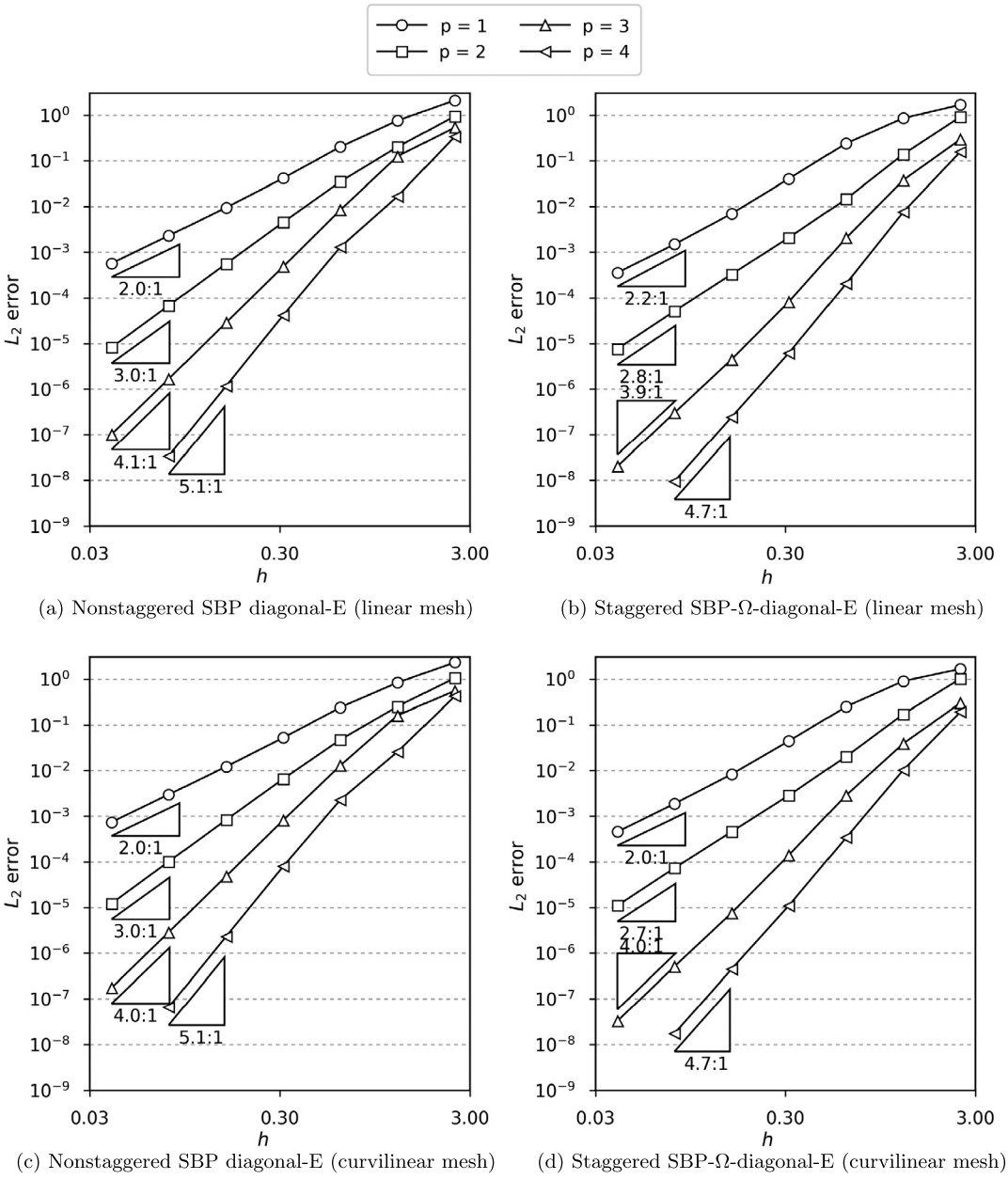

(a) Nonstaggered SBP diagonal-E (linear mesh)

(b) Staggered SBP-Ω-diagonal-E (linear mesh)

(c) Nonstaggered SBP diagonal-E (curvilinear mesh)

(d) Staggered SBP-Ω-diagonal-E (curvilinear mesh)

Fig. 5. Convergence studies.

Convergence plots for the collocated algorithm (using diagonal-E operators) and the staggered algorithm are displayed in Fig. 5. We observe that the obtained convergence rates are approximately $p+1$ and that the staggered algorithm results in more accurate solutions (we discuss efficiency in Section 6.3).

6.2. Discontinuous solution

To demonstrate the entropy conservative properties of the semidiscrete form, we consider a discontinuous initial condition and run our algorithm without interface dissipation. At the continuous level, shocks lead to a decrease in the integral of the mathematical entropy; however, our entropy conservative scheme has no mechanism for dissipation and therefore, entropy will remain constant. To verify that this is the case, we use the 20×20 rectangular linear element mesh and the initial condition (see Fig. 7a)

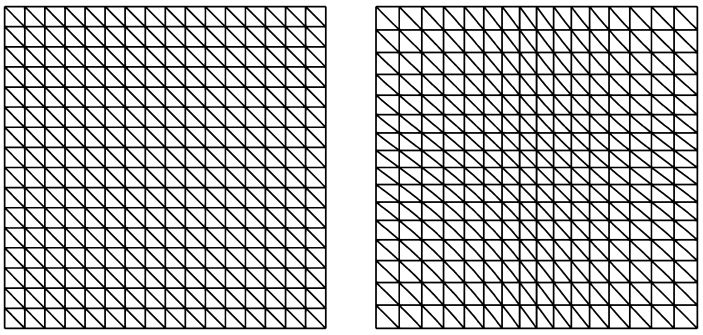

(a) Linear mesh (b) Curvilinear mesh

Fig. 6. Meshes for the Euler vortex propagation problem.

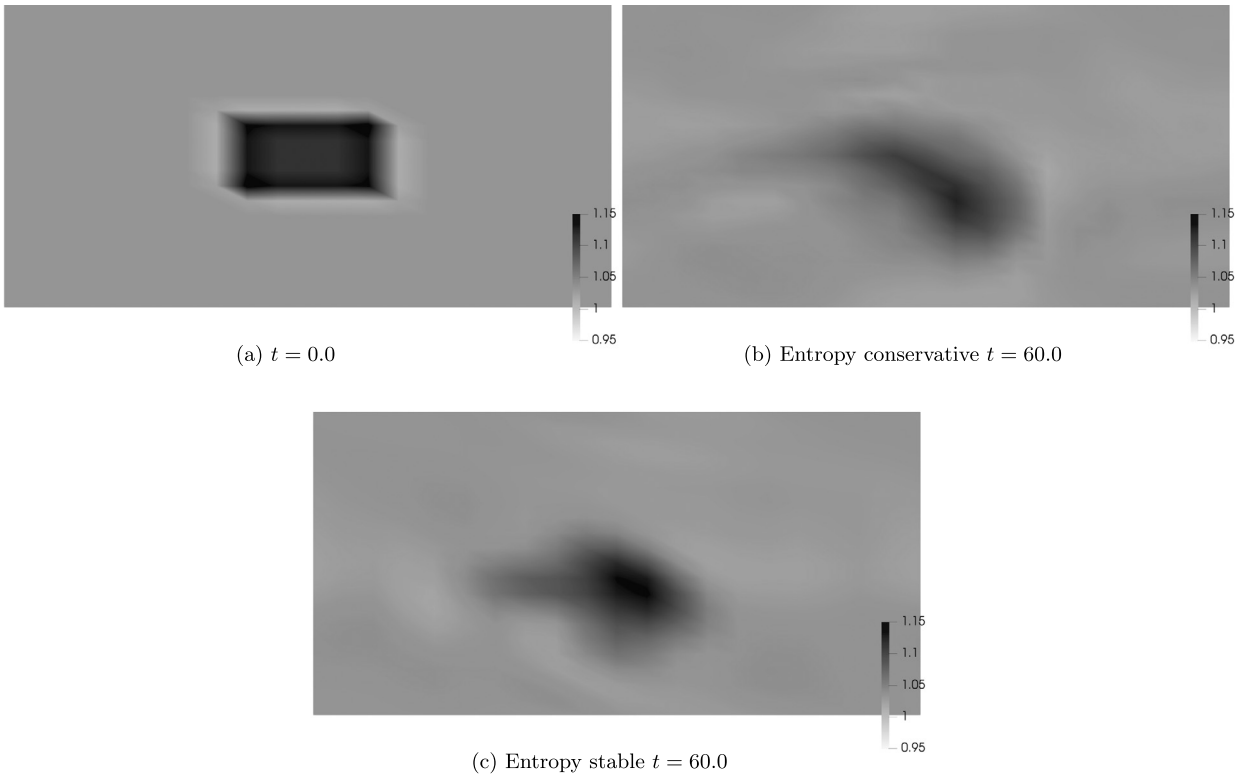

(a) $t = 0.0$ (b) Entropy conservative $t = 60.0$

(c) Entropy stable $t = 60.0$

Fig. 7. Discontinuous solution density.

$$\mathcal{U}(x, y) = \left[\rho, \rho u, \rho v, E\right]^T = \begin{cases} \left[1.1, 0.4, 0.4, 5.1\right]^T & \forall \quad 7.5 < x < 12.5, -1.25 < y < 1.25 \\ \left[1.0, 0.3, 0.3, 5.0\right]^T & \text{otherwise,} \end{cases}$$

on a domain $x \in [0, 20]$, $y \in [-5, 5]$. The problem is simulated to a maximum time of 60 nondimensional units using a CFL of 0.01 with periodic boundary conditions (see Fig. 7b and 7c). Figs. 8a and 8c plot

$$\sum_{\kappa=1}^{K} \boldsymbol{w}_\kappa^{\mathrm{T}} \mathrm{RHS}\left(\boldsymbol{u}_\kappa\right),$$

where $\mathrm{RHS}\left(\boldsymbol{u}_\kappa\right)$ is the spatial residual and $\boldsymbol{w}_\kappa$ is the vector of entropy variables. We see that the entropy remains small for all time verifying that the spatial discretization is entropy conserving (we have plotted $p = 1$ for an extended time range to verify that the spatial entropy is oscillating about machine zero, see Fig. 9). Figs. 8b and 8d plot the change in the discrete integral of the entropy function $\mathcal{S}$ over time, i.e.,

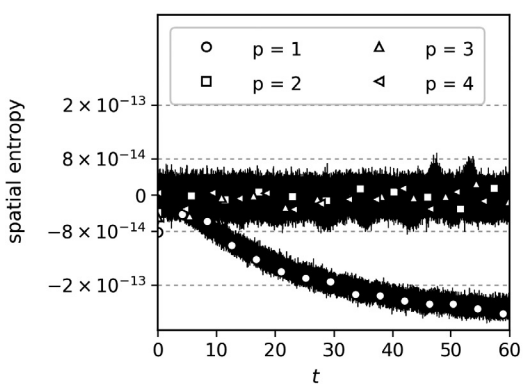

(a) Spatial contribution to entropy (linear mesh)

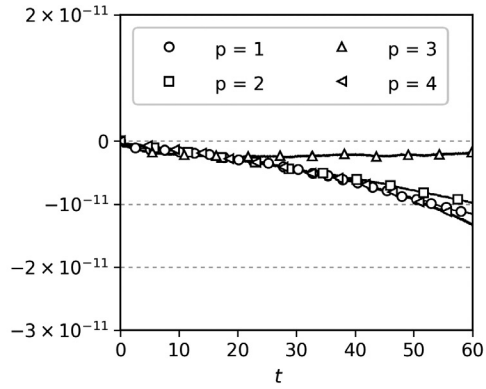

(b) Change in entropy from initial condition (linear mesh)

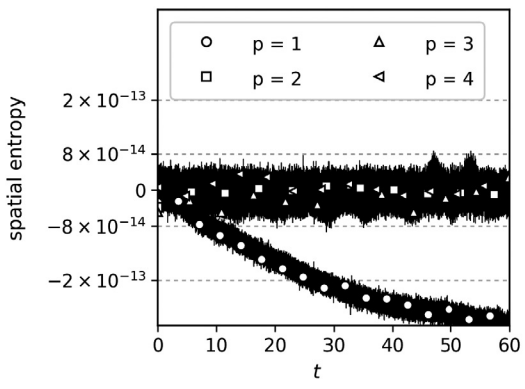

(c) Spatial contribution to entropy (curvilinear mesh)

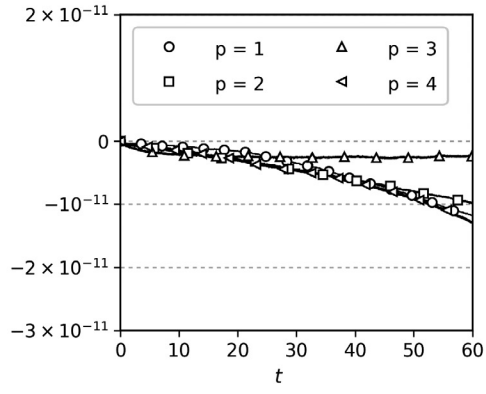

(d) Change in entropy from initial condition (curvilinear mesh)

Fig. 8. Discontinuous solution entropy conservative results.

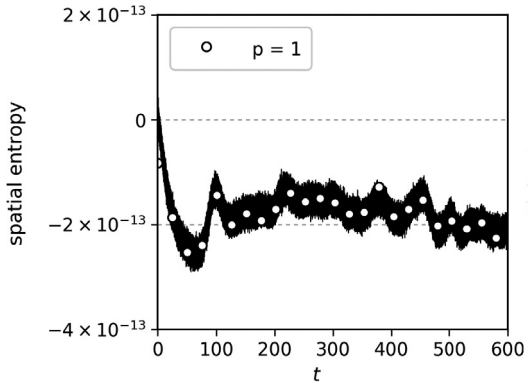

(a) Spatial contribution to entropy (linear mesh)

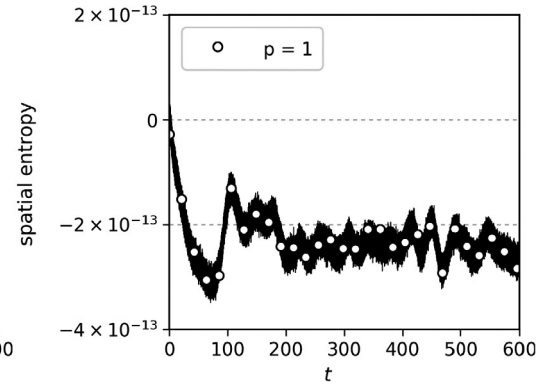

(b) Spatial contribution to entropy (curvilinear mesh)

Fig. 9. Spatial entropy for $p = 1$ extended run.

$$\text{change in entropy} \equiv \sum_{\kappa=1}^{K} \widetilde{\mathbf{1}}^{\mathrm{T}} \widetilde{\mathsf{H}} \widetilde{\mathsf{J}}_{\kappa} \left(\widetilde{\boldsymbol{s}}_{\kappa}(0) - \widetilde{\boldsymbol{s}}_{\kappa}(t) \right),$$

for which we see a decrease in the entropy, which results from the fact that the time discretization is not entropy conservative.

Table 1
Cost Comparison.

Operator degree	Cost per time step (s)		Ratio
	NonStaggered	Staggered	
$p = 1$	0.0353	0.0485	1.38
$p = 2$	0.0770	0.103	1.34
$p = 3$	0.150	0.255	1.70
$p = 4$	0.307	0.375	1.22

Table 2
Maximum stable time-step comparison.

Operator degree	NonStaggered Δt	Staggered Δt	Ratio
$p = 1$	0.0449	0.0525	1.17
$p = 2$	0.0225	0.0285	1.27
$p = 3$	0.0136	0.0150	1.10
$p = 4$	0.00971	0.0122	1.15

Table 3
Cost per time unit.

Operator degree	Ratio
$p = 1$	1.18
$p = 2$	1.06
$p = 3$	1.54
$p = 4$	1.06

6.3. Cost comparison

To assess the efficiency of the staggered grid algorithm, as compared to the collocated algorithm, we use the data from the 6th mesh (128^2 elements) of the problem in 6.1. The computations were performed with version 0.5 of the code developed in the lab of the fourth author, which can be found at: https://github.com/OptimalDesignLab/PDESolver.jl. The code is written in Julia, version 0.4, which uses the LLVM compiler, version 3.3. Individual components of the code have been benchmarked against C implementations in order to verify the performance is competitive. The timing studies were done on 3 nodes of a cluster, where each node has 2 Intel Xeon E5-2650 processors and 128 GB of system memory. The nodes are connected via 56 Gb FDR Infiniband, and OpenMPI version 2.0.2 is used for all parallel communications. Table 1 gives the cost per time step of the two algorithms. As anticipated, the staggered-grid algorithm is more costly but by less than a factor of 2.

However, as displayed in Table 2, this cost is partially or fully offset by the fact that a larger time step can be taken. The maximum stable timestep was computed using a binary search algorithm for CFL $\in [0.1, 5.0]$. If a run failed to complete or the final solution contained Inf or NaN, the CFL was considered unstable.

Finally, Table 3 gives the ratio of the staggered and the collocated algorithms to integrate one time unit if each algorithm is run at the maximum stable timestep. We see that for degree 1 and 3 operators, the algorithm is somewhat more expensive. While for even degree operators, the algorithm has comparable cost. Moreover, for degree 3 and 4, the algorithm is almost an order of magnitude more accurate (see Fig. 5), which gives strong indication that the staggered algorithm is more efficient.

While our numerical experiments have focused on explicit time marching, they demonstrate that the error in the staggered algorithm is at worst the same as the collocated algorithm; this means, all else equal, that for implicit schemes the staggered algorithm might be an attractive alternative to the collocated algorithm as a result of the significant reduction in DOFs.

7. Conclusions

We extend the entropy conservative/stable staggered grid tensor-product algorithm of Parsani et al. [1] to multidimensional SBP discretizations. We prove that under mild restrictions interpolation operators that preserve the SBP property exist. The resulting algorithm is shown to be entropy conservative/stable and elementwise conservative for curvilinear meshes. While the staggering incurs additional computational cost this is partially or fully offset by an improved CFL condition and increased accuracy for all polynomials considered except $p = 2$. The staggered grid algorithm is competitive for explicit time marching and in addition should be well suited for implicit time marching as it reduces the DOFs per element for each polynomial degree, while only using pointwise coupling between elements (typically not possible for minimum node SBP operators). Moreover, the pointwise coupling allows for the use of existing entropy stable numerical boundary conditions.

Appendix A. Recast of the semi-discrete form

In order to increase efficiency, at the cost of memory, we construct Cartesian derivatives as

$$\overline{\mathsf{D}}_{x_m} \equiv \frac{1}{2}\overline{\mathsf{H}}^{-1}\sum_{l=1}^{3}\left(\overline{\mathsf{A}}_{\kappa}^{l,m}\overline{\mathsf{Q}}_{\xi_l} - \overline{\mathsf{Q}}_{\xi_l}^{\mathrm{T}}\overline{\mathsf{A}}_{\kappa}^{l,m} + \sum_{\gamma\subset\partial\hat{\Omega}_\kappa}\overline{\mathsf{R}}_{\gamma\kappa}^{\mathrm{T}}\overline{\mathsf{N}}_{\xi_l,\gamma}\overline{\mathsf{B}}_{\gamma}\overline{\mathsf{A}}_{\gamma}^{l,m}\overline{\mathsf{R}}_{\gamma\kappa}\right),$$

then the algorithm (15) takes the form

$$\overline{\widetilde{\mathsf{H}}}\frac{\mathrm{d}\overline{\widetilde{\mathsf{J}}}_{\kappa}\widetilde{\boldsymbol{u}}_{\kappa}}{\mathrm{d}t} + \overline{\mathsf{I}}_{\mathrm{S2F}}^{\mathrm{T}}\sum_{m=1}^{3}\overline{\mathsf{S}}_{x_m}\circ\mathsf{F}_m\left(\boldsymbol{u}_{\kappa},\boldsymbol{u}_{\kappa}\right)\overline{\mathbf{1}} = -\overline{\mathsf{I}}_{\mathrm{S2F}}\sum_{\gamma\subset\partial\hat{\Omega}_\kappa}\sum_{l,m=1}^{3}\overline{\mathsf{E}}_{\xi_l,m,\gamma}^{\kappa,\nu}\circ\mathsf{F}_m(\boldsymbol{u}_{\kappa},\boldsymbol{u}_{\nu})\overline{\mathbf{1}},$$

which has a weak-form interpretation (see REFs. [4,43]).

Appendix B. Entropy conservation proof

The semidiscrete entropy conservation analysis follows step by step that for the continuous problem. First, we multiply (15) by $\widetilde{\boldsymbol{w}}_{\kappa}^{\mathrm{T}}\overline{\widetilde{\mathsf{H}}}$, where $\widetilde{\boldsymbol{w}}_{\kappa}$ is the vector of discrete entropy variables — this is equivalent to multiplying by the entropy variables and integrating over the domain. Doing so results in

$$\begin{aligned}&\widetilde{\boldsymbol{w}}_{\kappa}^{\mathrm{T}}\overline{\widetilde{\mathsf{H}}}\frac{\mathrm{d}\widetilde{\boldsymbol{u}}_{\kappa}}{\mathrm{d}t} + \widetilde{\boldsymbol{w}}_{\kappa}^{\mathrm{T}}\overline{\mathsf{I}}_{\mathrm{S2F}}^{\mathrm{T}}\sum_{l,m=1}^{3}\left(\overline{\mathsf{Q}}_{\xi_l}\mathsf{A}_{\kappa}^{l,m} + \mathsf{A}_{\kappa}^{l,m}\overline{\mathsf{Q}}_{\xi_l}\right)\circ\mathsf{F}_m\left(\boldsymbol{u}_{\kappa},\boldsymbol{u}_{\kappa}\right)\overline{\mathbf{1}}\\ &= \widetilde{\boldsymbol{w}}_{\kappa}^{\mathrm{T}}\overline{\mathsf{I}}_{\mathrm{S2F}}^{\mathrm{T}}\sum_{l,m=1}^{3}\left(\overline{\mathsf{E}}_{\xi_l}\mathsf{A}_{\kappa}^{l,m}\right)\circ\mathsf{F}_m\left(\boldsymbol{u}_{\kappa},\boldsymbol{u}_{\kappa}\right)\overline{\mathbf{1}} + \mathrm{CT},\end{aligned} \tag{B.1}$$

where we have used the interpolation condition (18) and

$$\mathrm{CT} \equiv -\widetilde{\boldsymbol{w}}_{\kappa}^{\mathrm{T}}\sum_{\gamma\subset\partial\hat{\Omega}_k}\sum_{l,m=1}^{3}\overline{\mathsf{E}}_{\xi_l,m,\gamma}^{\kappa,\nu}\circ\mathsf{F}_m(\boldsymbol{u}_{\kappa},\boldsymbol{u}_{\nu})\overline{\mathbf{1}}. \tag{B.2}$$

We proceed term by term; for the temporal term in (B.1), we apply the following manipulations:

$$\widetilde{\boldsymbol{w}}_{\kappa}^{\mathrm{T}}\overline{\widetilde{\mathsf{H}}}\frac{\mathrm{d}\widetilde{\boldsymbol{u}}_{\kappa}}{\mathrm{d}t} = \overline{\widetilde{\mathbf{1}}}^{\mathrm{T}}\overline{\widetilde{\mathsf{H}}}\,\mathrm{diag}\left(\widetilde{\boldsymbol{w}}_{\kappa}^{\mathrm{T}}\right)\frac{\mathrm{d}\widetilde{\boldsymbol{u}}_{\kappa}}{\mathrm{d}t} = \overline{\widetilde{\mathbf{1}}}^{\mathrm{T}}\overline{\widetilde{\mathsf{H}}}\frac{\mathrm{d}\widetilde{\boldsymbol{s}}_{\kappa}}{\mathrm{d}t}. \tag{B.3}$$

Next, we manipulate the volume terms on the left-hand side of (B.1). Defining $\boldsymbol{w}_{\kappa} \equiv \mathsf{I}_{\mathrm{S2F}}\widetilde{\boldsymbol{w}}_{\kappa}$ we have that

$$\mathrm{Vol} = \sum_{l,m=1}^{3}\boldsymbol{w}_{\kappa}^{\mathrm{T}}\left(\overline{\mathsf{Q}}_{\xi_l}\overline{\mathsf{A}}_{\kappa}^{l,m}\right)\circ\mathsf{F}_m\left(\boldsymbol{u}_{\kappa},\boldsymbol{u}_{\kappa}\right)\overline{\mathbf{1}} + \boldsymbol{w}_{\kappa}^{\mathrm{T}}\left(\overline{\mathsf{A}}_{\kappa}^{l,m}\overline{\mathsf{Q}}_{\xi_l}\right)\circ\mathsf{F}_m\left(\boldsymbol{u}_{\kappa},\boldsymbol{u}_{\kappa}\right)\overline{\mathbf{1}}. \tag{B.4}$$

Taking the transpose of the second term on the RHS of (B.4), we obtain

$$\mathrm{Vol} = \sum_{l,m=1}^{3}\boldsymbol{w}_{\kappa}^{\mathrm{T}}\left(\overline{\mathsf{Q}}_{\xi_l}\overline{\mathsf{A}}_{\kappa}^{l,m}\right)\circ\mathsf{F}_m\left(\boldsymbol{u}_{\kappa},\boldsymbol{u}_{\kappa}\right)\overline{\mathbf{1}} + \overline{\mathbf{1}}^{\mathrm{T}}\left[\overline{\mathsf{Q}}_{\xi_l}^{\mathrm{T}}\left(\overline{\mathsf{A}}_{\kappa}^{l,m}\right)^{\mathrm{T}}\right]\circ\mathsf{F}_m\left(\boldsymbol{u}_{\kappa},\boldsymbol{u}_{\kappa}\right)^{\mathrm{T}}\boldsymbol{w}_{\kappa}. \tag{B.5}$$

Noting that by symmetry $\mathsf{F}_m\left(\boldsymbol{u}_{\kappa},\boldsymbol{u}_{\kappa}\right)^{\mathrm{T}} = \mathsf{F}_m\left(\boldsymbol{u}_{\kappa},\boldsymbol{u}_{\kappa}\right)$, and $\left(\overline{\mathsf{A}}_{\kappa}^{l,m}\right)^{\mathrm{T}} = \overline{\mathsf{A}}_{\kappa}^{l,m}$, and substituting $\overline{\mathsf{Q}}_{\xi_l}^{\mathrm{T}} = -\overline{\mathsf{Q}}_{\xi_l} + \overline{\mathsf{E}}_{\xi_l}$ on the second term on the RHS of (B.5), equation (B.5) becomes

$$\mathrm{Vol} = \sum_{l,m=1}^{3}\boldsymbol{w}_{\kappa}^{\mathrm{T}}\left(\overline{\mathsf{Q}}_{\xi_l}\overline{\mathsf{A}}_{\kappa}^{l,m}\right)\circ\mathsf{F}_m\left(\boldsymbol{u}_{\kappa},\boldsymbol{u}_{\kappa}\right)\overline{\mathbf{1}} - \overline{\mathbf{1}}^{\mathrm{T}}\left(\overline{\mathsf{Q}}_{\xi_l}\overline{\mathsf{A}}_{\kappa}^{l,m}\right)\circ\mathsf{F}_m\left(\boldsymbol{u}_{\kappa},\boldsymbol{u}_{\kappa}\right)\boldsymbol{w}_{\kappa} + \overline{\mathbf{1}}^{\mathrm{T}}\left(\overline{\mathsf{E}}_{\xi_l}\overline{\mathsf{A}}_{\kappa}^{l,m}\right)\circ\mathsf{F}_m\left(\boldsymbol{u}_{\kappa},\boldsymbol{u}_{\kappa}\right)\boldsymbol{w}_{\kappa}. \tag{B.6}$$

Applying Lemma 1, equation (B.6) reduces to

$$\mathrm{Vol} = \sum_{l,m=1}^{3}\left(\boldsymbol{\psi}_m^{\kappa}\right)^{\mathrm{T}}\mathsf{Q}_{\xi_l}\mathsf{A}_{\kappa}^{l,m}\mathbf{1} - \mathbf{1}^{\mathrm{T}}\mathsf{Q}_{\xi_l}\mathsf{A}_{\kappa}^{l,m}\boldsymbol{\psi}_m^{\kappa} + \overline{\mathbf{1}}^{\mathrm{T}}\left(\overline{\mathsf{E}}_{\xi_l}\overline{\mathsf{A}}_{\kappa}^{l,m}\right)\circ\mathsf{F}_m\left(\boldsymbol{u}_{\kappa},\boldsymbol{u}_{\kappa}\right)\boldsymbol{w}_{\kappa}. \tag{B.7}$$

Substituting (B.3) and (B.7) into (B.1) and rearranging gives

$$\begin{aligned}\widetilde{\overline{\mathbf{1}}}^{\mathrm{T}}\widetilde{\overline{\mathsf{H}}}\frac{\mathrm{d}\widetilde{\boldsymbol{s}}_\kappa}{\mathrm{d}t} &= \sum_{l,m=1}^{3} -\left(\boldsymbol{\psi}_m^\kappa\right)^{\mathrm{T}}\mathsf{Q}_{\xi_l}\mathsf{A}_\kappa^{l,m}\mathbf{1} + \mathbf{1}^{\mathrm{T}}\mathsf{Q}_{\xi_l}\mathsf{A}_\kappa^{l,m}\boldsymbol{\psi}_m^\kappa \\ &+ \sum_{l,m=1}^{3}\left[\boldsymbol{w}_\kappa\left(\overline{\mathsf{E}}_{\xi_l}\overline{\mathsf{A}}_\kappa^{l,m}\right)\circ\mathsf{F}_m\left(\boldsymbol{u}_\kappa,\boldsymbol{u}_\kappa\right)\overline{\mathbf{1}} - \overline{\mathbf{1}}^{\mathrm{T}}\left(\overline{\mathsf{E}}_{\xi_l}\overline{\mathsf{A}}_\kappa^{l,m}\right)\circ\mathsf{F}_m\left(\boldsymbol{u}_\kappa,\boldsymbol{u}_\kappa\right)\boldsymbol{w}_\kappa\right] + \mathrm{CT}.\end{aligned} \tag{B.8}$$

Using Lemma 1 on the second sum of (B.8), we obtain

$$\widetilde{\overline{\mathbf{1}}}^{\mathrm{T}}\widetilde{\overline{\mathsf{H}}}\frac{\mathrm{d}\widetilde{\boldsymbol{s}}_\kappa}{\mathrm{d}t} = \sum_{l,m=1}^{3} -\left(\boldsymbol{\psi}_m^\kappa\right)^{\mathrm{T}}\mathsf{Q}_{\xi_l}\mathsf{A}_\kappa^{l,m}\mathbf{1} + \mathbf{1}^{\mathrm{T}}\mathsf{Q}_{\xi_l}\mathsf{A}_\kappa^{l,m}\boldsymbol{\psi}_m^\kappa + \sum_{l,m=1}^{3}\left[\left(\boldsymbol{\psi}_m^\kappa\right)^{\mathrm{T}}\mathsf{E}_{\xi_l}\mathsf{A}_\kappa^{l,m}\mathbf{1} - \mathbf{1}^{\mathrm{T}}\mathsf{E}_{\xi_l}\mathsf{A}_\kappa^{l,m}\boldsymbol{\psi}_m^\kappa\right] + \mathrm{CT}. \tag{B.9}$$

We expand the second the term on the RHS as

$$\mathbf{1}^{\mathrm{T}}\mathsf{Q}_{\xi_l}\mathsf{A}_\kappa^{l,m}\boldsymbol{\psi}_m^\kappa = -\mathbf{1}^{\mathrm{T}}\mathsf{Q}_{\xi_l}^{\mathrm{T}}\mathsf{A}_\kappa^{l,m}\boldsymbol{\psi}_m^\kappa + \mathbf{1}^{\mathrm{T}}\mathsf{E}_{\xi_l}\mathsf{A}_\kappa^{l,m}\boldsymbol{\psi}_m^\kappa = \mathbf{1}^{\mathrm{T}}\mathsf{E}_{\xi_l}\mathsf{A}_\kappa^{l,m}\boldsymbol{\psi}_m^\kappa,$$

where we have used the fact that $\mathbf{1}^{\mathrm{T}}\mathsf{Q}_{\xi_l} = \mathbf{0}$. Finally noting that $\mathsf{Q}_{\xi_l}^{\mathrm{T}} = -\mathsf{Q}_{\xi_l} + \mathsf{E}_{\xi_l}$ (B.9) reduces to

$$\widetilde{\overline{\mathbf{1}}}^{\mathrm{T}}\widetilde{\overline{\mathsf{H}}}\frac{\mathrm{d}\widetilde{\boldsymbol{s}}_\kappa}{\mathrm{d}t} = \sum_{l,m=1}^{3}\left(\boldsymbol{\psi}_m^\kappa\right)^{\mathrm{T}}\mathsf{Q}_{\xi_l}^{\mathrm{T}}\mathsf{A}_\kappa^{l,m}\mathbf{1} + \mathrm{CT}. \tag{B.10}$$

To simplify the analysis of the CT coupling terms (see (B.2)) on the right-hand side of (B.10), we consider one common surface between two elements and the contributions for one (l,m) combination from the elements on either side of this surface. Thus, we have the terms

$$\begin{aligned}&\mathrm{CT}_{l,m}^\kappa + \mathrm{CT}_{l,m}^\nu \equiv -\left(\boldsymbol{w}_\kappa^{\mathrm{T}}\overline{\mathsf{E}}_{\xi_l,m,\gamma}^{\kappa,\nu}\circ\mathsf{F}_m\left(\boldsymbol{u}_\kappa,\boldsymbol{u}_\nu\right)\overline{\mathbf{1}} + \boldsymbol{w}_\nu^{\mathrm{T}}\overline{\mathsf{E}}_{\xi_l,m,\gamma}^{\nu,\kappa}\circ\mathsf{F}_m\left(\boldsymbol{u}_\nu,\boldsymbol{u}_\kappa\right)\overline{\mathbf{1}}\right) = \\ &-\left(\boldsymbol{w}_\kappa^{\mathrm{T}}\overline{\mathsf{E}}_{\xi_l,m,\gamma}^{\kappa,\nu}\circ\mathsf{F}_m\left(\boldsymbol{u}_\kappa,\boldsymbol{u}_\nu\right)\overline{\mathbf{1}} + \overline{\mathbf{1}}^{\mathrm{T}}\left(\overline{\mathsf{E}}_{\xi_l,m,\gamma}^{\nu,\kappa}\right)^{\mathrm{T}}\circ\mathsf{F}_m\left(\boldsymbol{u}_\kappa,\boldsymbol{u}_\nu\right)\boldsymbol{w}_\nu\right),\end{aligned} \tag{B.11}$$

where the equality results from the fact that the transpose of a scalar is equal to itself and the symmetry of the dyadic flux matrix. Using (2), we obtain from (B.11)

$$\mathrm{CT}_{l,m}^\kappa + \mathrm{CT}_{l,m}^\nu = -\left(\boldsymbol{w}_\kappa^{\mathrm{T}}\overline{\mathsf{E}}_{\xi_l,m,\gamma}^{\kappa,\nu}\circ\mathsf{F}_m\left(\boldsymbol{u}_\kappa,\boldsymbol{u}_\nu\right)\overline{\mathbf{1}} - \overline{\mathbf{1}}^{\mathrm{T}}\overline{\mathsf{E}}_{\xi_l,m,\gamma}^{\kappa,\nu}\circ\mathsf{F}_m\left(\boldsymbol{u}_\kappa,\boldsymbol{u}_\nu\right)\boldsymbol{w}_\nu\right). \tag{B.12}$$

Using Lemma 1, we obtain from (B.12)

$$\mathrm{CT}_{l,m}^\kappa + \mathrm{CT}_{l,m}^\nu = -\left(\boldsymbol{\psi}_m^\kappa\right)^{\mathrm{T}}\mathsf{E}_{\xi_l,m,\gamma}^{\kappa,\nu}\mathbf{1} + \mathbf{1}^{\mathrm{T}}\mathsf{E}_{\xi_l,m,\gamma}^{\kappa,\nu}\boldsymbol{\psi}_m^\nu = -\left(\boldsymbol{\psi}_m^\kappa\right)^{\mathrm{T}}\mathsf{E}_{\xi_l,m,\gamma}^{\kappa,\nu}\mathbf{1} - \left(\boldsymbol{\psi}_m^\nu\right)^{\mathrm{T}}\mathsf{E}_{\xi_l,m,\gamma}^{\nu,\kappa}\mathbf{1}, \tag{B.13}$$

where the last equality follows from using (2). What (B.13) demonstrates is that we can decouple the surface coupling terms and analyze entropy conservation element by element.

Performing an identical set of manipulations on each coupling surface term and examining the contributions to the κth element, we obtain from (B.10)

$$\widetilde{\overline{\mathbf{1}}}^{\mathrm{T}}\widetilde{\overline{\mathsf{H}}}\frac{\mathrm{d}\widetilde{\boldsymbol{s}}_\kappa}{\mathrm{d}t} = \sum_{l,m=1}^{3}\left(\boldsymbol{\psi}_m^\kappa\right)^{\mathrm{T}}\mathsf{Q}_{\xi_l}^{\mathrm{T}}\mathsf{A}_\kappa^{l,m}\mathbf{1} - \sum_{\gamma\subset\partial\hat{\Omega}_\kappa}\sum_{l,m=1}^{3}\left(\boldsymbol{\psi}_m^\kappa\right)^{\mathrm{T}}\mathsf{E}_{\xi_l,m,\gamma}^{\kappa,\nu}\mathbf{1}$$

thus,

$$\widetilde{\overline{\mathbf{1}}}^{\mathrm{T}}\widetilde{\overline{\mathsf{H}}}\frac{\mathrm{d}\widetilde{\boldsymbol{s}}_\kappa}{\mathrm{d}t} = 0,$$

if

$$\sum_{l=1}^{3}\mathsf{Q}_{\xi_l}^{\mathrm{T}}\mathsf{A}_\kappa^{l,m}\mathbf{1} = \sum_{\gamma\subset\partial\hat{\Omega}_\kappa}\sum_{l=1}^{3}\mathsf{E}_{\xi_l,m,\gamma}^{\kappa,\nu}\mathbf{1}, \quad m = 1,2,3. \tag{B.14}$$

What is hidden in (B.14) is a discretization, in some sense, of the metric identities (5). This can be more clearly seen by using the SBP property $\mathsf{Q}_{\xi_l}^{\mathrm{T}} = -\mathsf{Q}_{\xi_l} + \mathsf{E}_{\xi_l}$ and multiplying by $-\mathsf{H}^{-1}$, which gives

$$\sum_{l=1}^{3}\mathsf{D}_{\xi_l}\mathsf{A}_\kappa^{l,m}\mathbf{1} = \mathsf{H}^{-1}\left(\sum_{l=1}^{3}\mathsf{E}_{\xi_l}\mathbf{1} - \sum_{\gamma\subset\partial\hat{\Omega}_\kappa}\sum_{l=1}^{3}\mathsf{E}_{\xi_l,m,\gamma}^{\kappa,\nu}\mathbf{1}\right), \quad m = 1,2,3. \tag{B.15}$$

Appendix C. Elementwise conservation

In the following subsections, we prove the various requirements for elementwise conservation given in Section 5.2 under the assumptions given in Theorem 8.

C.1. Telescoping flux form

The telescoping flux form is obtained by discretely integrating the semidiscrete form of each of the conservation laws over each element. To do so, we multiply the scalar semidiscrete forms obtained from (15) by $\widetilde{\mathbf{1}}^{\mathrm{T}}\widetilde{\mathsf{H}}$, which after using the properties of the interpolation operators, $\widetilde{\mathbf{1}}^{\mathrm{T}}\widetilde{\mathsf{H}}\mathsf{I}_{\mathrm{F2S}}\mathsf{H}^{-1} = \mathbf{1}^{\mathrm{T}}$, gives

$$\widetilde{\mathbf{1}}^{\mathrm{T}}\widetilde{\mathsf{H}}\widetilde{\mathsf{J}}_{\kappa}\frac{\mathrm{d}\boldsymbol{u}_{\kappa}^{(i)}}{\mathrm{d}t} + \mathbf{1}^{\mathrm{T}}\sum_{l,m=1}^{3}\left(\mathsf{Q}_{\xi_l}\mathsf{A}_{\kappa}^{l,m} + \mathsf{A}_{\kappa}^{l,m}\mathsf{Q}_{\xi_l}\right)\circ\mathsf{F}_m^{(i)}\left(\boldsymbol{u}_{\kappa},\boldsymbol{u}_{\kappa}\right)\mathbf{1} = \mathbf{1}^{\mathrm{T}}\sum_{l,m=1}^{3}\mathsf{E}_{\xi_l}\mathsf{A}_{\kappa}^{l,m}\circ\mathsf{F}_m^{(i)}\mathbf{1} - \mathbf{1}^{\mathrm{T}}\boldsymbol{CT}, \tag{C.1}$$

where $\boldsymbol{CT}$ are the coupling terms. Using the symmetry of $\mathsf{F}_m^{(i)}\left(\boldsymbol{u}_{\kappa},\boldsymbol{u}_{\kappa}\right)$, E_{ξ_l} and $\mathsf{A}_{\kappa}^{l,m}$, we have that

$$\mathbf{1}^{\mathrm{T}}\mathsf{E}_{\xi_l}\mathsf{A}_{\kappa}^{l,m}\circ\mathsf{F}_m^{(i)}\mathbf{1} = \frac{1}{2}\mathbf{1}^{\mathrm{T}}\mathsf{E}_{\xi_l}\mathsf{A}_{\kappa}^{l,m}\circ\mathsf{F}_m^{(i)}\mathbf{1} + \frac{1}{2}\mathbf{1}^{\mathrm{T}}\mathsf{A}_{\kappa}^{l,m}\mathsf{E}_{\xi_l}\circ\mathsf{F}_m^{(i)}\mathbf{1},$$

and therefore, C.1 reduces to

$$\widetilde{\mathbf{1}}^{\mathrm{T}}\widetilde{\mathsf{H}}\widetilde{\mathsf{J}}_{\kappa}\frac{\mathrm{d}\boldsymbol{u}_{\kappa}^{(i)}}{\mathrm{d}t} + \mathbf{1}^{\mathrm{T}}\sum_{l,m=1}^{3}\left(\mathsf{S}_{\xi_l}\mathsf{A}_{\kappa}^{l,m} + \mathsf{A}_{\kappa}^{l,m}\mathsf{S}_{\xi_l}\right)\circ\mathsf{F}_m^{(i)}\left(\boldsymbol{u}_{\kappa},\boldsymbol{u}_{\kappa}\right)\mathbf{1} = -\mathbf{1}^{\mathrm{T}}\boldsymbol{CT}.$$

The matrix $\left(\mathsf{S}_{\xi_l}\mathsf{A}_{\kappa}^{l,m} + \mathsf{A}_{\kappa}^{l,m}\mathsf{S}_{\xi_l}\right)\circ\mathsf{F}_m^{(i)}\left(\boldsymbol{u}_{\kappa},\boldsymbol{u}_{\kappa}\right)$ is skew-symmetric, thus, after expanding the coupling terms and rearranging, we are left with

$$\widetilde{\mathbf{1}}^{\mathrm{T}}\widetilde{\mathsf{H}}\widetilde{\mathsf{J}}_{\kappa}\frac{\mathrm{d}\boldsymbol{u}_{\kappa}^{(i)}}{\mathrm{d}t} + \sum_{l,m}\sum_{\gamma=1}^{\Gamma}\mathbf{1}^{\mathrm{T}}\mathsf{E}_{\xi_l}^{\gamma,\kappa}\circ\mathsf{F}_m^{(i)}\left(\boldsymbol{u}_{\kappa},\boldsymbol{u}_{\nu}\right)\mathbf{1} = 0,$$

which is in the form (21) where we identify

$$\overline{\boldsymbol{u}}_{\kappa}(i) \equiv \widetilde{\mathbf{1}}^{\mathrm{T}}\widetilde{\mathsf{H}}\widetilde{\mathsf{J}}_{\kappa}\boldsymbol{u}_{\kappa}^{(i)},$$

$$\boldsymbol{g}_{\kappa}^{\gamma}(i) \equiv \sum_{l,m=1}^{3}\mathbf{1}^{\mathrm{T}}\mathsf{E}_{\xi_l,m,\gamma}^{\kappa,\nu}\circ\mathsf{F}_m^{(i)}\left(\boldsymbol{u}_{\kappa},\boldsymbol{u}_{\nu}\right)\mathbf{1}, \quad 1,2,\ldots,5.$$

What we now need to show is that the flux at the element boundaries is unique, or equivalently, that the contributions from two abutting elements cancel. To show this, we take the sum of two coupling terms

$$\mathbf{1}^{\mathrm{T}}\boldsymbol{CT}_{\kappa}^{l,m} + \mathbf{1}^{\mathrm{T}}\boldsymbol{CT}_{\nu}^{l,m} = \mathbf{1}^{\mathrm{T}}\mathsf{E}_{\xi_l,m,\gamma}^{\kappa,\nu}\circ\mathsf{F}_m^{(i)}\left(\boldsymbol{u}_{\kappa},\boldsymbol{u}_{\nu}\right)\mathbf{1} + \mathbf{1}^{\mathrm{T}}\mathsf{E}_{\xi_l,m,\gamma}^{\nu,\kappa}\circ\mathsf{F}_m^{(i)}\left(\boldsymbol{u}_{\nu},\boldsymbol{u}_{\kappa}\right)\mathbf{1}.$$

Taking the transpose of the second term, using the symmetry of the flux function matrix and the assumption that $\left(\mathsf{E}_{\xi_l,m,\gamma}^{\kappa,\nu}\right)^{\mathrm{T}} = -\mathsf{E}_{\xi_l,m,\gamma}^{\nu,\kappa}$, we see that the terms cancel.

C.2. Consistency

In the theorem, we assume that the coupling terms satisfy the consistency condition (this follows from Theorem 6) and therefore, we need only show that the generalized conserved quantity satisfies the consistency condition. This follows immediately because $\widetilde{\mathsf{H}}$ is at least a degree $2p-1$ approximation to the L^2 inner product, that is for scalar functions $\mathcal{V}$ and $\mathcal{U}$

$$\boldsymbol{v}^{\mathrm{T}}\widetilde{\mathsf{H}}\boldsymbol{u} = \int_{\hat{\Omega}}\mathcal{V}\mathcal{U}\mathrm{d}\hat{\Omega} + \mathcal{O}\left(h^{2p}\right).$$

Thus, for a constant state $\mathcal{U}_c$, $\boldsymbol{u}_{\kappa}^{(i)} = \mathbf{1}\mathcal{U}_c(i)$ and we therefore have that

$$\overline{\boldsymbol{u}}_{\kappa}(i) = \widetilde{\mathbf{1}}^{\mathrm{T}}\widetilde{\mathsf{H}}\widetilde{\mathsf{J}}_{\kappa}\widetilde{\mathbf{1}}\mathcal{U}_{\kappa}(i) = \left[\int_{\hat{\Omega}_{\kappa}}\mathcal{J}_{\kappa}\mathrm{d}\hat{\Omega} + \mathcal{O}\left(h^{2p}\right)\right]\mathcal{Q}_c(i).$$

C.3. Boundedness

The bounds on the generalized conserved quantities can be shown as follows:

$$\begin{aligned}\left|\overline{\boldsymbol{u}}_\kappa(i)-\overline{\boldsymbol{v}}_\kappa(i)\right| &= \left|\widetilde{\mathbf{1}}^{\mathrm{T}}\widetilde{\mathsf{H}}\widetilde{\mathsf{J}}_\kappa\left(\boldsymbol{u}_\kappa^{(i)}-\boldsymbol{v}_\kappa^{(i)}\right)\right| = \left|\sum_{j=1}^{n_\kappa}\widetilde{\mathsf{H}}(j,j)\left(\boldsymbol{u}_\kappa^{(i)}(j)-\boldsymbol{v}_\kappa^{(i)}(j)\right)\right| \\ &\leq \sum_{j=1}^{n_\kappa}\widetilde{\mathsf{H}}(j,j)\left|\left(\boldsymbol{u}_\kappa^{(i)}(j)-\boldsymbol{v}_\kappa^{(i)}(j)\right)\right| \\ &\leq C\max_{j=1,\ldots,n_\kappa}\left(\left|\boldsymbol{u}_\kappa^{(i)}-\boldsymbol{v}_\kappa^{(i)}\right|\right) = C\left\|\boldsymbol{u}_\kappa^{(i)}-\boldsymbol{v}_\kappa^{(i)}\right\|_{L^\infty}.\end{aligned}$$

The generalized flux is constructed from linear combinations of two-point flux functions; for the Ismail-Roe flux, these have been shown to be continuously differentiable (see Crean et al. [4]) and are therefore bounded in the L^∞ norm.

C.4. Global conservation

Global conservation follows via the fact that the norm matrix is an approximation to the L^2 inner product; thus,

$$\sum_{\kappa=1}^{K}\overline{\boldsymbol{u}}_\kappa(i) = \sum_{\kappa=1}^{K}\widetilde{\mathbf{1}}^{\mathrm{T}}\widetilde{\mathsf{H}}\widetilde{\mathsf{J}}_\kappa\boldsymbol{u}_\kappa^{(i)} = \sum_{\kappa=1}^{K}\int_{\hat{\Omega}_\kappa}\boldsymbol{\mathcal{Q}}(i)\mathcal{J}_\kappa\mathrm{d}\hat{\Omega}+\mathcal{O}\left(h^{2p}\right) = \int_{\Omega}\boldsymbol{\mathcal{Q}}_i\mathrm{d}\Omega+\mathcal{O}\left(h^{2p}\right).$$

Appendix D. Existence of the interpolation operators

We start by assuming that the matrix $\widetilde{\mathsf{V}}_p$ has full column rank and note that V_p has full column rank as it supports a degree p differentiation operator. Next, we consider the augmented accuracy conditions on $\mathsf{I}_{\mathrm{S2F}}$:

$$\mathsf{I}_{\mathrm{S2F}}\left[\widetilde{\mathsf{V}}_p,\widetilde{\mathsf{W}}\right] = \left[\mathsf{V}_p,\mathsf{W}\right]. \tag{D.1}$$

We choose $\widetilde{\mathsf{W}}$ such that $\left[\widetilde{\mathsf{V}}_p,\widetilde{\mathsf{W}}\right]$ is invertible, which can always be done (our approach to choosing $\widetilde{\mathsf{W}}$ is detailed in Section 4.2), and therefore, we obtain that

$$\mathsf{I}_{\mathrm{S2F}} = \left[\mathsf{V}_p,\mathsf{W}\right]\left[\widetilde{\mathsf{V}}_p,\widetilde{\mathsf{W}}\right]^{-1}, \tag{D.2}$$

which is the form proposed in (11).

Next, we solve for $\mathsf{I}_{\mathrm{F2S}}$ from the stability condition in (10), which gives

$$\mathsf{I}_{\mathrm{F2S}} = \widetilde{\mathsf{H}}^{-1}\mathsf{I}_{\mathrm{S2F}}^{\mathrm{T}}\mathsf{H}. \tag{D.3}$$

We must now show that this form of $\mathsf{I}_{\mathrm{F2S}}$ satisfies the accuracy conditions in (10) (we do so for $\hat{p}=p-1$). As for $\mathsf{I}_{\mathrm{S2F}}$, we consider the augmented accuracy conditions

$$\mathsf{I}_{\mathrm{F2S}}\left[\mathsf{V}_{p-1},\mathsf{X}\right] = \left[\widetilde{\mathsf{V}}_{p-1},\widetilde{\mathsf{X}}\right]. \tag{D.4}$$

Substituting (D.2) into (D.3) and substituting the result into (D.4) results in

$$\widetilde{\mathsf{H}}^{-1}\left[\widetilde{\mathsf{V}}_p,\widetilde{\mathsf{W}}\right]^{-\mathrm{T}}\left[\mathsf{V}_p,\mathsf{W}\right]^{\mathrm{T}}\mathsf{H}\left[\mathsf{V}_{p-1},\mathsf{X}\right] = \left[\widetilde{\mathsf{V}}_{p-1},\widetilde{\mathsf{X}}\right]. \tag{D.5}$$

Left multiplying (D.5) by $\left[\widetilde{\mathsf{V}}_p,\widetilde{\mathsf{W}}\right]^{\mathrm{T}}\widetilde{\mathsf{H}}$, and converting to matrix notation gives

$$\begin{bmatrix}\mathsf{V}_p^{\mathrm{T}}\mathsf{H}\mathsf{V}_{p-1} & \mathsf{V}_p^{\mathrm{T}}\mathsf{H}\mathsf{X}\\ \mathsf{W}^{\mathrm{T}}\mathsf{H}\mathsf{V}_{p-1} & \mathsf{W}^{\mathrm{T}}\mathsf{H}\mathsf{X}\end{bmatrix} = \begin{bmatrix}\widetilde{\mathsf{V}}_p^{\mathrm{T}}\widetilde{\mathsf{H}}\widetilde{\mathsf{V}}_{p-1} & \widetilde{\mathsf{V}}_p^{\mathrm{T}}\widetilde{\mathsf{H}}\widetilde{\mathsf{X}}\\ \widetilde{\mathsf{W}}^{\mathrm{T}}\widetilde{\mathsf{H}}\widetilde{\mathsf{V}}_{p-1} & \widetilde{\mathsf{W}}^{\mathrm{T}}\widetilde{\mathsf{H}}\widetilde{\mathsf{X}}\end{bmatrix}, \tag{D.6}$$

which are conditions (12). Finally, we prove that the proposed solution satisfies (D.6). We see that under the assumption that $\mathsf{V}_p^{\mathrm{T}}\mathsf{H}\mathsf{V}_{p-1} = \widetilde{\mathsf{V}}_p^{\mathrm{T}}\widetilde{\mathsf{H}}\widetilde{\mathsf{V}}_{p-1}$, and choosing $\widetilde{\mathsf{X}}=0$ and $\mathsf{X}=0$, we need to only show that the choice

$$\mathsf{W} = \left[\widetilde{\mathsf{W}}^{\mathrm{T}}\widetilde{\mathsf{H}}\widetilde{\mathsf{V}}_{p-1}\left(\mathsf{V}_p^{\mathrm{T}}\mathsf{V}_p\right)^{-1}\mathsf{V}_p^{\mathrm{T}}\mathsf{H}^{-1}\right]^{\mathrm{T}}, \tag{D.7}$$

satisfies the condition

$$\mathsf{W}^{\mathrm{T}}\mathsf{H}\mathsf{V}_{p-1} = \widetilde{\mathsf{W}}^{\mathrm{T}}\widetilde{\mathsf{H}}\widetilde{\mathsf{V}}_{p-1}, \tag{D.8}$$

which can easily be shown by substituting (D.7) into (D.8).

Appendix E. Proof of Corollary 2

It is easy to show that as constructed, I_{S2F} satisfies the accuracy conditions of (10). We now show that the resulting I_{F2S} satisfies the accuracy conditions

$$\begin{aligned}&\mathsf{I}_{F2S}\mathsf{V}_p = \widetilde{\mathsf{V}}_p\\ &\widetilde{\mathsf{H}}^{-1}\widetilde{\mathsf{V}}_p^{-\mathrm{T}}\mathsf{V}_p^{\mathrm{T}}\mathsf{H}\mathsf{V}_p = \widetilde{\mathsf{V}}_p.\end{aligned} \tag{E.1}$$

Multiplying both sides of the last equality in (E.1) by $\widetilde{\mathsf{V}}_p^{\mathrm{T}}\widetilde{\mathsf{H}}$ gives

$$\mathsf{V}_p^{\mathrm{T}}\mathsf{H}\mathsf{V}_p = \widetilde{\mathsf{V}}_p^{\mathrm{T}}\widetilde{\mathsf{H}}\widetilde{\mathsf{V}}_p,$$

which holds because both $\widetilde{\mathsf{H}}$ and H are at least degree $2p$ and therefore, I_{F2S} satisfies the accuracy conditions.

The proof of (13) proceeds as follows:

$$\mathsf{I}_{F2S}\mathsf{I}_{S2F} = \widetilde{\mathsf{H}}^{-1}\widetilde{\mathsf{V}}_p^{-\mathrm{T}}\mathsf{V}_p^{\mathrm{T}}\mathsf{H}\mathsf{V}_p\widetilde{\mathsf{V}}_p^{-1} = \mathsf{I}. \tag{E.2}$$

Left multiplying both sides of the last equality of (E.2) by $\widetilde{\mathsf{V}}_p^{\mathrm{T}}\widetilde{\mathsf{H}}$ and right multiplying by $\widetilde{\mathsf{V}}_p$ gives

$$\mathsf{V}_p^{\mathrm{T}}\mathsf{H}\mathsf{V}_p = \widetilde{\mathsf{V}}_p^{\mathrm{T}}\widetilde{\mathsf{H}}\widetilde{\mathsf{V}}_p,$$

which holds because both $\widetilde{\mathsf{H}}$ and H are at least degree $2p$ and therefore, $\mathsf{I}_{F2S}\mathsf{I}_{S2F} = \mathsf{I}$.

Appendix F. Free-stream preservation

To prove that the semidiscrete scheme preserves the free stream, we insert a constant state $\boldsymbol{\mathcal{U}} = \boldsymbol{\mathcal{U}}_c$ into the numerical scheme by using $\boldsymbol{u}_\kappa = \mathbf{1}\otimes\boldsymbol{\mathcal{U}}_c$. By symmetry and consistency, we have that

$$\mathsf{F}_m\left(\boldsymbol{u}_\kappa, \boldsymbol{u}_\kappa\right) = \mathbf{1}\mathbf{1}^{\mathrm{T}}\otimes\mathrm{diag}\left[\boldsymbol{\mathcal{F}}_m\left(\boldsymbol{\mathcal{U}}_c\right)\right].$$

We require the following property of the Hadamard product of tensor product matrices:

$$\left(\mathsf{A}_1\otimes\mathsf{A}_2\otimes\ldots\mathsf{A}_n\right)\circ\left(\mathsf{B}_1\otimes\mathsf{B}_2\otimes\ldots\mathsf{B}_n\right) = \left(\mathsf{A}_1\circ\mathsf{B}_1\right)\otimes\left(\mathsf{A}_2\circ\mathsf{B}_2\right)\otimes\ldots\left(\mathsf{A}_n\circ\mathsf{B}_n\right). \tag{F.1}$$

Substituting the constant state into (15) gives

$$\begin{aligned}&\frac{\mathrm{d}\overline{\widetilde{\mathsf{J}}}_\kappa\widetilde{\mathbf{1}}\otimes\boldsymbol{\mathcal{U}}_c}{\mathrm{d}t} + \overline{\mathsf{I}}_{F2S}\sum_{l,m=1}^{3}\left(\overline{\mathsf{D}}_{\xi_l}\overline{\mathsf{A}}_\kappa^{l,m} + \overline{\mathsf{A}}_\kappa^{l,m}\overline{\mathsf{D}}_{\xi_l}\right)\circ\left\{\mathbf{1}\mathbf{1}^{\mathrm{T}}\otimes\mathrm{diag}\left[\boldsymbol{\mathcal{F}}_m\left(\boldsymbol{\mathcal{U}}_c\right)\right]\right\}\mathbf{1}\otimes\mathbf{1}_5\\ &= \overline{\mathsf{I}}_{F2S}\overline{\mathsf{H}}^{-1}\sum_{l,m=1}^{3}\left(\overline{\mathsf{E}}_{\xi_l}\overline{\mathsf{A}}_\kappa^{l,m}\right)\circ\left\{\mathbf{1}\mathbf{1}^{\mathrm{T}}\otimes\mathrm{diag}\left[\boldsymbol{\mathcal{F}}_m\left(\boldsymbol{\mathcal{U}}_c\right)\right]\right\}\mathbf{1}\otimes\mathbf{1}_5\\ &- \overline{\mathsf{I}}_{F2S}\overline{\mathsf{H}}^{-1}\sum_{\gamma\subset\partial\hat{\Omega}_\kappa}\sum_{l,m=1}^{3}\overline{\mathsf{E}}_{\xi_l,m,\gamma}^{\kappa,\nu}\circ\left\{\mathbf{1}\mathbf{1}^{\mathrm{T}}\otimes\mathrm{diag}\left[\boldsymbol{\mathcal{F}}_m\left(\boldsymbol{\mathcal{U}}_c\right)\right]\right\}\mathbf{1}\otimes\mathbf{1}_5,\end{aligned} \tag{F.2}$$

Using the fact that the discrete operators are of the form $\overline{\mathsf{D}} = \mathsf{D}\otimes\mathsf{I}_5$ and properties (F.1), (F.2) reduces to

$$\begin{aligned}&\frac{\mathrm{d}\overline{\widetilde{\mathsf{J}}}_\kappa\widetilde{\mathbf{1}}\otimes\boldsymbol{\mathcal{U}}_c}{\mathrm{d}t} + \overline{\mathsf{I}}_{F2S}\sum_{l,m=1}^{3}\left\{\left[\left(\mathsf{D}_{\xi_l}\mathsf{A}_\kappa^{l,m} + \mathsf{A}_\kappa^{l,m}\mathsf{D}_{\xi_l}\right)\circ\mathbf{1}\mathbf{1}^{\mathrm{T}}\right]\mathbf{1}\right\}\otimes\left\{\mathsf{I}_5\circ\mathrm{diag}\left[\boldsymbol{\mathcal{F}}_m\left(\boldsymbol{\mathcal{U}}_c\right)\right]\right\}\\ &= \overline{\mathsf{I}}_{F2S}\overline{\mathsf{H}}^{-1}\sum_{l,m=1}^{3}\left\{\left[\left(\mathsf{E}_{\xi_l}\mathsf{A}_\kappa^{l,m}\right)\circ\mathbf{1}\mathbf{1}^{\mathrm{T}}\right]\mathbf{1}\right\}\otimes\left\{\mathsf{I}_5\circ\mathrm{diag}\left[\boldsymbol{\mathcal{F}}_m\left(\boldsymbol{\mathcal{U}}_c\right)\right]\right\}\\ &- \overline{\mathsf{I}}_{F2S}\overline{\mathsf{H}}^{-1}\sum_{\gamma\subset\partial\hat{\Omega}_\kappa}\sum_{l,m=1}^{3}\left[\left(\mathsf{E}_{\xi_l,m,\gamma}^{\kappa,\nu}\circ\mathbf{1}\mathbf{1}^{\mathrm{T}}\right)\mathbf{1}\right]\otimes\left\{\mathsf{I}_5\circ\mathrm{diag}\left[\boldsymbol{\mathcal{F}}_m\left(\boldsymbol{\mathcal{U}}_c\right)\right]\right\}.\end{aligned} \tag{F.3}$$

Using the fact that $\mathsf{D}\mathbf{1} = \mathbf{0}$ and after simplifying, we obtain

$$\frac{\mathrm{d}\bar{\widetilde{\mathsf{J}}}_\kappa \widetilde{\mathbf{1}} \otimes \boldsymbol{\mathcal{U}}_c}{\mathrm{d}t} + \bar{\mathsf{I}}_{\mathrm{F2S}} \sum_{l,m=1}^{3} \left(\mathsf{D}_{\xi_l} \mathsf{A}_\kappa^{l,m} \mathbf{1} \right) \otimes \left[\boldsymbol{\mathcal{F}}_m \left(\boldsymbol{\mathcal{U}}_c \right) \right] = \bar{\mathsf{I}}_{\mathrm{F2S}} \overline{\mathsf{H}}^{-1} \sum_{l,m=1}^{3} \left(\mathsf{E}_{\xi_l} \mathsf{A}_\kappa^{l,m} \mathbf{1} \right) \otimes \left[\boldsymbol{\mathcal{F}}_m \left(\boldsymbol{\mathcal{U}}_c \right) \right]$$
$$- \bar{\mathsf{I}}_{\mathrm{F2S}} \overline{\mathsf{H}}^{-1} \sum_{\gamma \subset \partial \hat{\Omega}_\kappa} \sum_{l,m=1}^{3} \left(\mathsf{E}_{\xi_l,m,\gamma}^{\kappa,\nu} \mathbf{1} \right) \otimes \left[\boldsymbol{\mathcal{F}}_m \left(\boldsymbol{\mathcal{U}}_c \right) \right]. \tag{F.4}$$

For free-stream preservation, all but the temporal terms must be zero; one solution is

$$\sum_{m=1}^{3} \mathsf{D}_{\xi_l} \mathsf{A}_\kappa^{l,m} \mathbf{1} = \mathsf{H}^{-1} \left(\sum_{m=1}^{3} \mathsf{E}_{\xi_l} \mathsf{A}_\kappa^{l,m} \mathbf{1} - \sum_{\gamma \subset \partial \hat{\Omega}_k} \sum_{l,m=1}^{3} \mathsf{E}_{\xi_l,m,\gamma}^{\kappa,\nu} \mathbf{1} \right),$$

which is identical to the conditions (17).

References

[1] M. Parsani, M.H. Carpenter, T.C. Fisher, E.J. Nielsen, Entropy stable staggered grid discontinuous spectral collocation methods of any order for the compressible Navier-Stokes equations, SIAM J. Sci. Comput. 38 (5) (2016) A3129–A3162.
[2] M.H. Carpenter, T.C. Fisher, E.J. Nielsen, S.H. Frankel, Entropy stable spectral collocation schemes for the Navier-Stokes equations: discontinuous interfaces, SIAM J. Sci. Comput. 36 (5) (2014) B835–B867.
[3] T. Chen, C.-W. Shu, Entropy stable high order discontinuous Galerkin methods with suitable quadrature rules for hyperbolic conservation laws, J. Comput. Phys. 345 (2017) 427–461.
[4] J. Crean, J.E. Hicken, D.C.D.R. Fernández, D.W. Zingg, M.H. Carpenter, Entropy-stable summation-by-parts discretization of the Euler equations on general curved elements, J. Comput. Phys. 356 (2018) 410–438.
[5] H.-O. Kreiss, J. Oliger, Comparison of accurate methods for the integration of hyperbolic equations, Tellus 24 (3) (1972) 199–215.
[6] B. Swartz, B. Wendroff, The relative efficiency of finite difference and finite element methods. I: Hyperbolic problems and splines, SIAM J. Numer. Anal. 11 (5) (1974) 979–993.
[7] D.C. Del Rey Fernández, J.E. Hicken, D.W. Zingg, Review of summation-by-parts operators with simultaneous approximation terms for the numerical solution of partial differential equations, Comput. Fluids 95 (22) (2014) 171–196.
[8] M. Svärd, J. Nordström, Review of summation-by-parts schemes for initial-boundary-value-problems, J. Comput. Phys. 268 (1) (2014) 17–38.
[9] M.H. Carpenter, D. Gottlieb, S. Abarbanel, Time-stable boundary conditions for finite-difference schemes solving hyperbolic systems: methodology and application to high-order compact schemes, J. Comput. Phys. 111 (2) (1994) 220–236.
[10] M.H. Carpenter, J. Nordström, D. Gottlieb, A stable and conservative interface treatment of arbitrary spatial accuracy, J. Comput. Phys. 148 (2) (1999) 341–365.
[11] J. Nordström, M.H. Carpenter, Boundary and interface conditions for high-order finite-difference methods applied to the Euler and Navier-Stokes equations, J. Comput. Phys. 148 (2) (1999) 621–645.
[12] J. Nordström, M.H. Carpenter, High-order finite-difference methods, multidimensional linear problems, and curvilinear coordinates, J. Comput. Phys. 173 (1) (2001) 149–174.
[13] M.H. Carpenter, J. Nordström, D. Gottlieb, Revisiting and extending interface penalties for multi-domain summation-by-parts operators, J. Sci. Comput. 45 (1) (June 2010) 118–150.
[14] E. Tadmor, The numerical viscosity of entropy stable schemes for systems of conservation laws I, Math. Comput. 49 (179) (July 1987) 91–103.
[15] E. Tadmor, Entropy stability theory for difference approximations of nonlinear conservation laws and related time-dependent problems, Acta Numer. 12 (2003) 451–512.
[16] U.S. Fjordholm, S. Mishra, E. Tadmor, Arbitrarily high-order accurate entropy stable essentially nonoscillatory schemes for systems of conservation laws, Commun. Comput. Phys. 50 (2) (2012) 554–573.
[17] D. Ray, P. Chandrashekar, U.S. Fjordhom, S. Mishra, Entropy stable scheme on two-dimensional unstructured grids for Euler equations, Commun. Comput. Phys. 19 (5) (2016) 1111–1140.
[18] T.C. Fisher, High-Order L^2 Stable Multi-Domain Finite Difference Method for Compressible Flows, Ph.D. thesis, Purdue University, August 2012.
[19] T.C. Fisher, M.H. Carpenter, J. Nordström, N.K. Yamaleev, Discretely conservative finite-difference formulations for nonlinear conservation laws in split form: theory and boundary conditions, J. Comput. Phys. 234 (1) (2013) 353–375.
[20] T.C. Fisher, M.H. Carpenter, High-order entropy stable finite difference schemes for nonlinear conservation laws: finite domains, J. Comput. Phys. 252 (2013) 518–557.
[21] J. Chan, On discretely entropy conservative and entropy stable discontinuous Galerkin methods, J. Comput. Phys. 362 (2018) 346–374.
[22] A.R. Winters, D. Derigs, G.J. Gassner, S. Walch, Uniquely defined entropy stable matrix dissipation operator for high Mach number ideal MHD and compressible Euler simulations, J. Comput. Phys. 332 (1) (2017) 274–289.
[23] D. Derigs, A.R. Winters, G.J. Gassner, S. Walch, A novel averaging technique for discrete entropy-stable dissipation operators for ideal MHD, J. Comput. Phys. 330 (1) (2017) 624–632.
[24] A.R. Winters, G.J. Gassner, Affordable, entropy conserving and entropy stable flux functions for the ideal MHD equations, J. Comput. Phys. 304 (1) (2016) 72–108.
[25] N. Wintermeyer, A.R. Winters, G.J. Gassner, D.A. Kopriva, An entropy stable nodal discontinuous Galerkin method for the two dimensional shallow water equations on unstructured curvilinear meshes with discontinuous bathymetry, J. Comput. Phys. 340 (1) (2017) 200–242.
[26] G.J. Gassner, A.R. Winters, D.A. Kopriva, A well balanced and entropy conservative discontinuous Galerkin spectral element method for the shallow water equations, Appl. Math. Comput. 272 (2) (2016) 291–308.
[27] A.R. Winters, G.J. Gassner, A comparison of two entropy stable discontinuous Galerkin spectral element approximations to the shallow water equations with non-constant topography, J. Comput. Phys. 301 (1) (2015) 357–376.
[28] L. Friedrich, G. Shnücke, A.R. Winters, D.C. Del Rey Fernández, G.J. Gassner, M.H. Carpenter, Entropy stable space-time discontinuous Galerkin schemes with summation-by-parts property for hyperbolic conservation laws, J. Sci. Comput. (2019), https://doi.org/10.1007/s10915-019-00933-2.
[29] T.J.R. Hughes, L.P. Franca, M. Mallet, A new finite element formulation for computational fluid dynamics, I: symmetric forms of the compressible Navier-Stokes equations and the second law of thermodynamics, Comput. Methods Appl. Mech. Eng. 54 (2) (1986) 223–234.
[30] G.S. Jiang, C.-W. Shu, On a cell entropy inequality for discontinuous Galerkin methods, Math. Comput. 62 (206) (1993).

[31] J.E. Hicken, D.C. Del Rey Fernández, D.W. Zingg, Multi-dimensional summation-by-parts operators: general theory and application to simplex elements, SIAM J. Sci. Comput. 38 (4) (2016) A1935–A1958.
[32] D.C. Del Rey Fernández, P.D. Boom, D.W. Zingg, A generalized framework for nodal first derivative summation-by-parts operators, J. Comput. Phys. 266 (1) (2014) 214–239.
[33] D.C. Del Rey Fernández, J.E. Hicken, D.W. Zingg, Simultaneous approximation terms for multidimensional summation-by-parts operators, J. Sci. Comput. 1 (75) (2018).
[34] J.E. Hicken, D.C. Del Rey Fernández, D.W. Zingg, Simultaneous approximation terms for multi-dimensional summation-by-parts operators, in: 46th AIAA Fluid Dynamics Conference, Washington, DC, June 2016, AIAA–2016–3971.
[35] R.J. LeVeque, Finite-Volume Methods for Hyperbolic Problems, Cambridge University Press, Cambridge, 2004.
[36] C.M. Dafermos, Hyperbolic Conservation Laws in Continuum Physics, Springer-Verlag, Berlin, 2010.
[37] M. Svärd, Weak solutions and convergent numerical schemes of modified compressible Navier-Stokes equations, J. Comput. Phys. 288 (C) (May 2015) 19–51.
[38] S.K. Godunov, An interesting class of quasilinear systems, Dokl. Akad. Nauk SSSR 139 (3) (1961) 521–523, English translation: Soviet Math. 2 (1961) 947–949.
[39] M.S. Mock, Systems of conservation laws of mixed type, J. Differ. Equ. 37 (1) (1980) 70–88.
[40] A. Harten, On the symmetric form of systems of conservation laws with entropy, J. Comput. Phys. 49 (1983) 151–164.
[41] F. Ismail, P.L. Roe, Affordable, entropy-consistent Euler flux functions II: entropy production at shocks, J. Comput. Phys. 228 (15) (2009) 5410–5436.
[42] P. Chandrashekar, Kinetic energy preserving and entropy stable finite volume schemes for compressible Euler and Navier-Stokes equations, Commun. Comput. Phys. 14 (5) (2013) 1252–1286.
[43] D.C. Del Rey Fernández, M.H. Carpenter, L. Fredrich, A.R. Winters, G.J.G.L. Dalcin, M. Parsani, Entropy Stable Non-conforming Discretizations With the Summation-by-Parts Property for Curvilinear Coordinates, NASA Technical Report, 2018.
[44] C. Shi, C.-W. Shu, On local conservation of numerical methods for conservation laws, Comput. Fluids 169 (4) (2018) 3–9.
[45] M.H. Carpenter, C.A. Kennedy, Fourth-Order 2N-Storage Runge-Kutta Schemes, Tech. rep., NASA, Nasa Langley Research Center, Hampton, Virginia, June 1994.
[46] M. Parsani, M. Carpenter, T. Fisher, E. Nielsen, Entropy stable staggered grid discontinuous spectral collocation methods of any order for the compressible Navier–Stokes equations, SIAM J. Sci. Comput. 38 (5) (2016) A3129–A3162.